

Runge-Kutta discontinuous Galerkin methods for the special relativistic magnetohydrodynamics

Jian Zhao

*HEDPS, CAPT & LMAM, School of Mathematical Sciences, Peking University,
Beijing 100871, P.R. China*

Huazhong Tang¹

*HEDPS, CAPT & LMAM, School of Mathematical Sciences, Peking University,
Beijing 100871, P.R. China; School of Mathematics and Computational Science,
Xiangtan University, Hunan Province, Xiangtan 411105, P.R. China*

Abstract

This paper develops P^K -based non-central and central Runge-Kutta discontinuous Galerkin (DG) methods with WENO limiter for the one- and two-dimensional special relativistic magnetohydrodynamical (RMHD) equations, $K = 1, 2, 3$. The non-central DG methods are locally divergence-free, while the central DG are “exactly” divergence-free but have to find two approximate solutions defined on mutually dual meshes. The adaptive WENO limiter first identifies the “troubled” cells by using a modified TVB minmod function, and then uses the WENO technique to locally reconstruct a new polynomial of degree $(2K + 1)$ inside the “troubled” cells replacing the DG solution by based on the cell average values of the DG solutions in the neighboring cells as well as the original cell averages of the “troubled” cells. The WENO limiting procedure does not destroy the locally or “exactly” divergence-free property of magnetic field and is only employed for finite “troubled” cells so that the computational cost can be as little as possible. Several test problems in one and two dimensions are solved by using our non-central and central Runge-Kutta DG methods with WENO limiter. The numerical results demonstrate that our methods are stable, accurate, and robust in resolving complex wave structures.

Key words: Discontinuous Galerkin method, WENO limiter, Runge-Kutta time discretization, relativistic magnetohydrodynamics.

1 Introduction

Relativistic hydrodynamics (RHD) or relativistic magnetohydrodynamics (RMHD) play major roles in astrophysics, nuclear physics, plasma physics and other fields. They are necessary in situations where the local velocity of the flow is close to the light speed in vacuum or where the local internal energy density is comparable (or larger) than the local rest mass density of the fluid. For example, in the formation of neutron stars and black holes, and the high-speed jet of physical phenomena, the relativistic effect can not be neglected so that the RHDs or RMHDs are needed. The dynamics of RMHD system requires solving highly nonlinear equations so that the analytic treatment of practical RMHD problems is extremely difficult. Numerical simulation has become an important way in studying RHDs and RMHDs. In the past few decades, significant progress is made and several numerical methods have been developed to investigate the RMHD equations.

The pioneering numerical work may date back to the finite difference code via artificial viscosity for the spherically symmetric general RHD equations in the Lagrangian coordinate [37,38]. Wilson first attempted to solve multi-dimensional RHD equations in the Eulerian coordinate by using the finite difference method with the artificial viscosity technique [53]. After that, a lot of modern shock-capturing methods in non relativistic hydrodynamics were extended to the RHD and RMHD equations. For example, some latest works are the adaptive moving mesh methods [22,23], second-order generalized problem schemes [61,62,55] and third-order GRP scheme [60], the locally evolution Galerkin method [59], approximate Riemann solvers based on the local linearization [27,26], TVD scheme [5], HLL scheme [64], HLLC schemes [39,24], the kinetic scheme [42], and adaptive mesh refinement methods [1,52] etc. Recently three physical-constraints-preserving (PCP) schemes were developed for the special RHD equations. They are the high-order accurate PCP finite difference weighted essentially non-oscillatory (WENO) schemes and discontinuous Galerkin (DG) methods proposed in [56,58,43]. Moreover, the set of admissible states and the PCP schemes of the ideal RMHDs was also studied for the first time in [57], where the importance of divergence-free fields was revealed in achieving PCP methods especially.

The magnetohydrodynamics mainly studies the interaction between magnetic field and conducting fluid. Compared with the RHD equations, the RMHD equations not only contain more number of the equations with complicated forms, but also an additional divergence-free constraint of magnetic field. Violating such constraint leads to non-physical plasma transport orthogonal to the magnetic field. Some special techniques must be employed to preserve that constraint. Up to now, three popular approaches have been suggested in the context of MHD equations. They are the eight-wave for-

Email addresses: `everease@163.com` (Jian Zhao), `hztang@math.pku.edu.cn` (Huazhong Tang).

¹ Corresponding author. Tel: +86-10-62757018; Fax: +86-10-62751801.

mulation of the MHD equations [41], the constrained transport method [20], and the projection method [9]. In the DG framework, locally divergence-free DG methods [30] and “exactly” divergence-free central DG methods [32] have been developed. All of the above works are on the non-relativistic MHD equations and some of them have been extended to the relativistic case.

The DG methods have been rapidly developed in recent decades and become a kind of important methods in computational fluid dynamics. It is easy to achieve high order accuracy, be suitable for parallel computing, and adapt to complex boundary. The DG method was first developed by Reed and Hill [45] to solve scalar, steady-state linear hyperbolic equation, but it had not been widely used. A major development of the DG methods was carried out by Cockburn and coworkers in a series of papers [15,14,13,11,17], where the DG spatial approximation was combined with explicit Runge-Kutta time discretization to develop the Runge-Kutta DG methods, and a general framework of DG methods was established for the nonlinear equation or system. The Runge-Kutta DG methods have gotten a wide range of research and application, such as the Euler equations [50,8,46], Maxwell equations [12], nonlinear Dirac equations [48] etc. Moreover, the DG methods have also been used to solve other partial differential equations, such as convection-diffusion type equation or system [6,16] and Hamilton-Jacobi equation [25,29,33] etc. The readers are referred to the review article [18].

The central DG methods [35] were developed by combining the DG methods and central scheme [34] and found two approximate solutions defined on mutually dual meshes. Although two approximate solutions are redundant, the numerical flux may be avoided due to the use of the solution on the dual grid to calculate the flux at the cell interface. It is one of the advantages of the central scheme. Because the central DG methods can be regarded as a variant of traditional/no-central DG methods, they keep many advantages of no-central DG methods, such as compact stencil and parallel implementation etc. Moreover, the central DG methods allow a larger CFL number than no-central DG methods and may reduce numerical oscillations for some problems. Up to now, the central DG methods have also been used to solve the Euler equations [35], the ideal magneto-hydrodynamical equations [32,31], the special relativistic hydrodynamical equations [67,58] and so on.

When the strong discontinuity appears in the solution, the numerical oscillations in the DG solutions should be suppressed after each Runge-Kutta inner stage or after some complete Runge-Kutta steps by using the nonlinear limiter, which is a commonly used technique in the modern shock-capturing methods for hyperbolic conservation laws. The commonly used limiter is the minmod limiter, which limits the slope of solution such that the values of limited solution in the cell falls in the certain interval determined by the cell average values of neighboring cells. It has good robustness but is only first-order accurate near extreme points. Cockburn et al. gave modified TVB minmod limiter and applied it to the non-central DG methods. The modified TVB minmod limiter does

not limit the solution near extreme points by choosing a parameter M , thus it does not destroy the accuracy of DG methods near the extreme point. In general, for nonlinear equation, the parameter M is dependent on the problem. Moreover, for $K \geq 3$, the accuracy of P^K -based DG methods may still be destroyed because more than three of the higher order moments will be set to zero by the modified TVB minmod limiter. Besides that commonly used limiter, some other limiters are proposed, such as the moment based limiters [8] and its improvement [28] etc. Those limiters may suppress numerical oscillations near the discontinuity, however, the accuracy of DG methods can be reduced in some region.

In the modern shock-capturing methods, the ENO (non-oscillatory essentially) and WENO methods have been widely used [49] and are more robust than the slope limiter methodology, especially for high order schemes. An attempt has been made to use an ENO or WENO methodology as limiter for the DG methods [44, 69, 68]. The WENO limiter first identifies the “troubled” cells by using a modified TVB minmod function, and then a new polynomial inside the “troubled” cells is locally reconstructed to replace the DG solution by using the WENO technique and the cell average values of the DG solutions in the neighboring cells as well as the original cell averages of the “troubled” cells. Because the WENO limiter is only employed for finite “troubled” cells, the computational cost can be as little as possible.

The aim of this paper develops P^K -based non-central and central Runge-Kutta discontinuous Galerkin (DG) methods with WENO limiter for the one- and two-dimensional special RMHD equations, $K = 1, 2, 3$. The former is locally divergence-free, while the latter is “exactly” divergence-free. It is organized as follows. Section 2 introduces the special RMHD equations and calculation of eigenvalues. Sections 3 and 4 give P^K -based locally and “exactly” divergence-free DG methods with WENO limiter for the special RMHD equations, respectively, $K = 1, 2, 3$. Section 5 conducts several numerical experiments to demonstrate the accuracy and efficiency of the proposed DG methods. Conclusions are given in Section 6.

2 Relativistic magnetohydrodynamical equations

This section introduces the relativistic magnetohydrodynamical (RMHD) equations and calculation of the eigenvalues for the Jacobian matrix.

The RMHDs is investigating the interaction between magnetic field and conducting fluid. In the covariant form, the four-dimensional space-time RMHD equations may be

written as follows [2,3]

$$\begin{cases} \partial_\alpha(\rho u^\alpha) = 0, \\ \partial_\alpha\left((\rho h + |\mathbf{b}|^2)u^\alpha u^\beta - b^\alpha b^\beta + p_{tot}g^{\alpha\beta}\right) = 0, \\ \partial_\alpha(u^\alpha b^\beta - u^\beta b^\alpha) = 0, \end{cases} \quad (2.1)$$

which stand for the laws of local baryon number conservation and energy-momentum conservation, and the induction equation for the magnetic field. In (2.1), the Greek indices α and β run from 0 to 3, $\partial_\alpha = \partial_{x^\alpha}$ denotes the covariant derivative with $x^\alpha = (ct, x_1, x_2, x_3)^T$, $u^\alpha = \gamma(c, v_1, v_2, v_3)^T$ stands for the four-velocity vector, $\gamma = 1/\sqrt{1 - |\mathbf{v}|^2/c^2}$ is the Lorentz factor with the fluid velocity vector $\mathbf{v} := (v_1, v_2, v_3)^T$, $g^{\alpha\beta}$ denotes the metric tensor, which is restricted to the Minkowski tensor in this paper, i.e. $(g^{\alpha\beta})_{4 \times 4} = \text{diag}\{-1, 1, 1, 1\}$, the relativistic enthalpy h is defined by

$$h = 1 + \frac{e}{c^2} + \frac{p}{\rho c^2},$$

where e is the specific internal energy and related to other thermodynamic or state variables such as the temperature, the pressure, the volume, or the internal energy etc. by the equation of state (EOS). The simplest EOS is the ideal gas law given by

$$p = (\Gamma - 1)\rho e, \quad (2.2)$$

where Γ is the adiabatic index (also ratio of specific heats). In comparison to the RHD equations, the RMHD equations (2.1) involve the four-magnetic field vector

$$b^\alpha = \gamma \left(\frac{\mathbf{v} \cdot \mathbf{B}}{c}, B_1/\gamma^2 + v_1 \frac{\mathbf{v} \cdot \mathbf{B}}{c^2}, B_2/\gamma^2 + v_2 \frac{\mathbf{v} \cdot \mathbf{B}}{c^2}, B_3/\gamma^2 + v_3 \frac{\mathbf{v} \cdot \mathbf{B}}{c^2} \right)^T,$$

where $\mathbf{B} = (B_1, B_2, B_3)$ is the magnetic field, the total pressure p_{tot} consists of the gas pressure p and magnetic pressure p_m , that is, $p_{tot} = p + p_m$, here the magnetic pressure $p_m = \frac{1}{2}b^\alpha b_\alpha$, $b_\alpha := g_{\alpha\beta}b^\beta$, and $g_{\alpha\beta}$ is the inverse of metric matrix $g^{\alpha\beta}$.

Throughout this paper, units in which the speed of light is equal to one will be used so that

$$\begin{aligned} x^\alpha &= (t, x_1, x_2, x_3)^T, \quad u^\alpha = \gamma(1, v_1, v_2, v_3)^T, \\ b^\alpha &= \gamma \left(\mathbf{v} \cdot \mathbf{B}, B_1/\gamma^2 + v_1(\mathbf{v} \cdot \mathbf{B}), B_2/\gamma^2 + v_2(\mathbf{v} \cdot \mathbf{B}), B_3/\gamma^2 + v_3(\mathbf{v} \cdot \mathbf{B}) \right)^T. \end{aligned}$$

It is obvious from (2.1) that in modeling flow at speeds where relativistic effects become important, space and time become intrinsically coupled and the governing equations of the ideal RMHDs become more complicated. Nonetheless, it is still possible to write (2.1) into a first-order system of time evolution equations in some fixed reference frame

(i.e. the so-called lab frame) as follows

$$\nabla \cdot \mathbf{B} = 0, \quad (2.3)$$

$$\frac{\partial \mathbf{U}}{\partial t} + \sum_{i=1}^3 \frac{\partial \mathbf{F}_i(\mathbf{U})}{\partial x_i} = 0, \quad (2.4)$$

where \mathbf{U} is the conservative vector, \mathbf{F}_i is the flux in the x_i direction, $i = 1, 2, 3$, and their expressions are given by

$$\begin{aligned} \mathbf{U} &= \left(D, m_1, m_2, m_3, B_1, B_2, B_3, E \right)^T, \\ \mathbf{F}_1 &= \left(Dv_1, m_1v_1 - B_1b_1/\gamma + p_{tot}, m_2v_1 - B_1b_2/\gamma, \right. \\ &\quad \left. m_3v_1 - B_1b_3/\gamma, 0, B_2v_1 - B_1v_2, B_3v_1 - B_1v_3, m_1 \right)^T, \\ \mathbf{F}_2 &= \left(Dv_2, m_1v_2 - B_2b_1/\gamma, m_2v_2 - B_2b_2/\gamma + p_{tot}, \right. \\ &\quad \left. m_3v_2 - B_2b_3/\gamma, B_1v_2 - B_2v_1, 0, B_3v_2 - B_2v_3, m_2 \right)^T, \\ \mathbf{F}_3 &= \left(Dv_3, m_1v_3 - B_3b_1/\gamma, m_2v_3 - B_3b_2/\gamma, \right. \\ &\quad \left. m_3v_3 - B_3b_3/\gamma + p_{tot}, B_1v_3 - B_3v_1, B_2v_3 - B_3v_2, 0, m_3 \right)^T, \end{aligned}$$

here $D = \rho\gamma$, $m_i = (\rho h\gamma^2 + |\mathbf{B}|^2)v_i - (\mathbf{v} \cdot \mathbf{B})B_i$, and $E = Dh\gamma - p_{tot} + |\mathbf{B}|^2$ denote the mass, x_i -momentum, and energy densities in the lab frame, respectively. Eq. (2.3) is a divergence-free constraint on the magnetic field, and the solutions of (2.4) should satisfy such constraint at any time. Numerically preserving such condition is very non-trivial but important for the robustness of numerical scheme, and has to be respected. In physics, numerically incorrect magnetic field topologies may lead to nonphysical plasma transport orthogonal to the magnetic field. The condition (2.3) is also very crucial for the stability of induction equation. The existing numerical experiments in the non-relativistic MHD case have also indicated that violating the divergence free condition of magnetic field may lead to numerical instability and nonphysical or inadmissible solutions.

The flux \mathbf{F}_i in (2.4) cannot be explicitly expressed as a function of \mathbf{U} but can be cast into an explicit function of primitive variable vector $\mathbf{V} := (\rho, v_1, v_2, v_3, B_1, B_2, B_3, p)^T$. Thus if giving the value of \mathbf{U} , then one has to get the value of \mathbf{V} in order to calculate \mathbf{F}_i . Up to now, several approaches have been suggested to recover the primitive variables from the conservative vector in the literature, e.g. six numerical approaches discussed in [40]. The approach in [26] is used here. If introducing an auxiliary variable $\theta := \rho h\gamma^2 > 0$ and denoting $\mathbf{m} := (m_1, m_2, m_3)^T$, then it is easy to prove the following identities

$$\mathbf{v} \cdot \mathbf{B} = \theta^{-1}(\mathbf{m} \cdot \mathbf{B}),$$

and

$$\mathbf{v} = \frac{\mathbf{m} + \theta^{-1}(\mathbf{m} \cdot \mathbf{B})\mathbf{B}}{\theta + |\mathbf{B}|^2},$$

$$p_m = \frac{b^\alpha b_\alpha}{2} = \frac{1}{2} \left(\frac{|\mathbf{B}|^2}{\gamma^2} + \frac{(\mathbf{m} \cdot \mathbf{B})^2}{\theta^2} \right),$$

where the Lorentz factor γ is expressed as follows

$$\gamma = (1 - |\mathbf{v}|^2)^{-\frac{1}{2}} = \left(1 - \frac{\theta^2 |\mathbf{m}|^2 + 2\theta(\mathbf{m} \cdot \mathbf{B})^2 + (\mathbf{m} \cdot \mathbf{B})^2 |\mathbf{B}|^2}{\theta^2(\theta + |\mathbf{B}|^2)^2} \right)^{-\frac{1}{2}},$$

and the density ρ and pressure p are written as

$$\rho = \frac{D}{\gamma}, \quad p = \frac{\Gamma - 1}{\Gamma} \left(\frac{\theta}{\gamma^2} - \frac{D}{\gamma} \right).$$

Substituting the above equations into the energy density expression $E = \rho h \gamma^2 - p - p_m + |\mathbf{B}|^2$ gives a nonlinear equation with respect to θ as follows

$$\theta - \frac{\Gamma - 1}{\Gamma} \left(\frac{\theta}{\gamma^2} - \frac{D}{\gamma} \right) - \frac{1}{2} \left(\frac{|\mathbf{B}|^2}{\gamma^2} + \frac{(\mathbf{m} \cdot \mathbf{B})^2}{\theta^2} \right) + |\mathbf{B}|^2 - E = 0, \quad (2.5)$$

which may be solved by any standard root finding algorithm such as the Newton-Raphson method. Once θ is found to some accuracy, the Lorentz factor γ , velocity \mathbf{v} , density ρ , and gas pressure p can be orderly calculated.

Remark 2.1 *It is not difficult to know that $\theta_{min} := \theta^* \leq \theta < \Gamma E =: \theta_{max}$, where θ^* satisfies $\gamma(\theta^*) = 1 + \epsilon$, and ϵ is a small positive number. Thus in practical computations, the initial guess for the Newton-Raphson method of (2.5) may be chosen as $(\theta_{min} + \theta_{max})/2$, and the iteration number is generally less than 8.*

The characteristic structure of the RMHD equations was first studied in [3]. The eigenvalues and eigenvectors of the Jacobian matrix is needed in our numerical methods for (2.4). Here gives the calculation of eigenvalues. Without loss of generality, consider x_1 -split system. Because the component of \mathbf{F}_1 corresponding to B_1 is zero, $B_1 = \text{const}$ and x_1 -split system consists of the following seven equations

$$\frac{\partial \mathbf{U}}{\partial t} + \frac{\partial \mathbf{F}_1(\mathbf{U})}{\partial x_1} = 0, \quad (2.6)$$

where

$$\mathbf{U} = \left(D, m_1, m_2, m_3, B_2, B_3, E \right)^T,$$

$$\mathbf{F}_1 = \left(Dv_1, m_1v_1 - B_1b_1/\gamma + p_{tot}, m_2v_1 - B_1b_2/\gamma, \right. \\ \left. m_3v_1 - B_1b_3/\gamma, B_2v_1 - B_1v_2, B_3v_1 - B_1v_3, m_1 \right)^T.$$

The eigensystem of the Jacobian matrix $\partial \mathbf{F}_1 / \partial \mathbf{U}$ can be found by slightly modifying the eigen-system for the one-dimensional RMHD equations, which have seven waves: two Alfvén, two fast and two slow magnetosonic waves (also magnetoacoustic wave), and an entropy wave, whose the speeds are denoted by $\lambda_1^{a,\pm}$, $\lambda_1^{f,\pm}$, $\lambda_1^{s,\pm}$, and λ_1^e , separately. They satisfy [4]

$$\lambda_1^{f,-} \leq \lambda_1^{a,-} \leq \lambda_1^{s,-} \leq \lambda_1^e \leq \lambda_1^{s,+} \leq \lambda_1^{a,+} \leq \lambda_1^{f,+},$$

where the speed of entropy wave λ_1^e is equal to v_1 , speeds of two Alfvén wave satisfy the following quadratic equation

$$(\rho h + |\mathbf{b}|^2) \gamma^2 (v_1 - \lambda)^2 - (b^1 - b^0 \lambda)^2 = 0,$$

which can be directly solved by the root formula of quadratic equation with one unknown, while speeds of four magnetoacoustic wave satisfy the following quartic equation [39]

$$\rho h (1 - c_s^2) a^4 = (1 - \lambda^2) \left[(|\mathbf{b}|^2 + \rho h c_s^2) a^2 - c_s^2 (b^1 - \lambda b^0)^2 \right], \quad (2.7)$$

where $a = \gamma(\lambda - v_1)$, and c_s is the sound speed and becomes $c_s = \sqrt{\Gamma p / (\rho h)}$ for the perfect gas. In some cases, Eq. (2.7) may be simplified and solved. In the following it is discussed in three cases.

- If the fluid velocity $\mathbf{v} = \mathbf{0}$, then Eq. (2.7) reduces to

$$(\rho h + |\mathbf{b}|^2) \lambda^4 - (|\mathbf{b}|^2 + \rho h c_s^2 + B_1^2 c_s^2) \lambda^2 + c_s^2 B_1^2 = 0,$$

which can be solved by the root formula of quadratic equation with one unknown to get the value of λ^2 , and so will the value of λ .

- If the normal component of magnetic field is zero, that is, $B_1 = 0$, then Eq. (2.7) degenerate into

$$a_2 \lambda^2 + a_1 \lambda + a_0 = 0, \quad (2.8)$$

where the coefficients are given by

$$a_2 = \rho h \left[c_s^2 + \gamma^2 (1 - c_s^2) \right] + |\mathbf{b}|^2 - c_s^2 (\mathbf{v} \cdot \mathbf{B})^2,$$

$$a_1 = -2 \rho h \gamma^2 v_1 (1 - c_s^2),$$

$$a_0 = \rho h \left[-c_s^2 + \gamma^2 v_1^2 (1 - c_s^2) \right] - |\mathbf{b}|^2 + c_s^2 (\mathbf{v} \cdot \mathbf{B})^2.$$

Eq. (2.8) can also be solved by the root formula of quadratic equation with one unknown.

- In addition to the above two cases, one has to solve the original quartic equation (2.7), which is solved by using the analytic formula in our work, certainly can also be solved by some iterative method.

It has been seen that the expressions of eigenvalues of Jacobian matrix of (2.4) is more complicated than the non-relativistic case, the calculation of corresponding eigenvectors is very complicated and may be obtained by the matrix transformation [4].

3 Locally divergence-free DG methods

Because the divergence-free constraint (2.3) of the magnetic field is natural for one-dimensional RMHD equations, no special numerical treatment is required for such constraint and thus the one-dimensional RMHD equations may be directly solved by using the non-central or central DG methods described in [66, 65], they are not repeated here.

This section gives locally divergence-free DG methods for the two-dimensional RMHD equations

$$\nabla \cdot \mathbf{B} = 0, \quad (x, y) \in \Omega, \quad (3.1)$$

$$\frac{\partial \mathbf{U}}{\partial t} + \frac{\partial \mathbf{F}_1(\mathbf{U})}{\partial x} + \frac{\partial \mathbf{F}_2(\mathbf{U})}{\partial y} = 0, \quad (x, y) \in \Omega, \quad (3.2)$$

on the rectangular mesh $\{e_{j,k}, \forall j, k \in \mathbb{Z}\}$, where

$$\begin{aligned} \mathbf{U} &= \left(D, m_x, m_y, m_z, B_x, B_y, B_z, E \right)^T, \\ \mathbf{F}_1 &= \left(Dv_x, m_x v_x - B_x b_x / \gamma + p_{tot}, m_y v_x - B_x b_y / \gamma, \right. \\ &\quad \left. m_z v_x - B_x b_z / \gamma, 0, B_y v_x - B_x v_y, B_z v_x - B_x v_z, m_x \right)^T, \\ \mathbf{F}_2 &= \left(Dv_y, m_x v_y - B_y b_x / \gamma, m_y v_y - B_y b_y / \gamma + p_{tot}, \right. \\ &\quad \left. m_z v_y - B_y b_z / \gamma, B_x v_y - B_y v_x, 0, B_z v_y - B_y v_z, m_y \right)^T, \end{aligned}$$

and $e_{j,k} = (x_{j-\frac{1}{2}}, x_{j+\frac{1}{2}}) \times (y_{k-\frac{1}{2}}, y_{k+\frac{1}{2}})$.

The conservative vector \mathbf{U} is divided into two parts as follows

$$\mathbf{R} = (D, m_x, m_y, m_z, B_z, E)^T, \quad \mathbf{Q} = (B_x, B_y)^T,$$

and similarly the flux vector \mathbf{F}_i is also written into $\mathbf{F}_i^R(\mathbf{U})$ and $\mathbf{F}_i^Q(\mathbf{U})$. After that, the RMHD equations (3.2) may be recast into

$$\frac{\partial \mathbf{R}}{\partial t} + \frac{\partial \mathbf{F}_1^R(\mathbf{U})}{\partial x} + \frac{\partial \mathbf{F}_2^R(\mathbf{U})}{\partial y} = 0, \quad (3.3)$$

$$\frac{\partial \mathbf{Q}}{\partial t} + \frac{\partial \mathbf{F}_1^Q(\mathbf{U})}{\partial x} + \frac{\partial \mathbf{F}_2^Q(\mathbf{U})}{\partial y} = 0. \quad (3.4)$$

The aim of locally divergence-free DG methods is to find an approximation \mathbf{U}_h of \mathbf{U} , where the approximations of \mathbf{R} and \mathbf{Q} are denoted by \mathbf{R}_h and \mathbf{Q}_h , respectively, but the spatial discretizations for \mathbf{R} and \mathbf{Q} are different, see below.

3.1 Spatial approximation

The divergence-free constraint of magnetic field is not needed in solving the system (3.3) for \mathbf{R} by using the DG methods, thus the DG approximation of the system (3.3) is similar to that for the RHD equations, see [66, 65], and will be omitted here.

Let us discuss the spatial discretization of the governing equations for the dependent variable \mathbf{Q} . The DG methods find the approximate solution \mathbf{Q}_h such that for any t , \mathbf{Q}_h belongs to the following finite dimensional function space

$$\mathbf{M}_h := \left\{ \mathbf{v}(\mathbf{x}) \in \mathbf{W}^K(e_{j,k}), \quad \mathbf{x} = (x, y) \in e_{j,k}, \forall j, k \right\},$$

where

$$\mathbf{W}^K(e_{j,k}) := \left\{ \mathbf{v} = \left(v_1(\mathbf{x}), v_2(\mathbf{x}) \right)^T \mid v_1(\mathbf{x}), v_2(\mathbf{x}) \in \mathbb{P}^K(e_{j,k}), \frac{\partial v_1}{\partial x} + \frac{\partial v_2}{\partial y} = 0 \right\}.$$

The basis functions of $\mathbf{W}^K(e_{j,k})$ may be obtained by calculating the curl of any vector function whose components are basis functions of $\mathbb{P}^{K+1}(e_{j,k})$, thus the dimension of $\mathbf{W}^K(e_{j,k})$ is equal to $D_W = (K+1)(K+4)/2$. The following lists a set of basis function of $\mathbf{W}^K(e_{j,k})$ for the case of $K = 3$

$$\begin{aligned} \varphi_{j,k}^{(0)}(x, y) &= \begin{pmatrix} 0 \\ 1 \end{pmatrix}, \quad \varphi_{j,k}^{(1)}(x, y) = \begin{pmatrix} 1 \\ 0 \end{pmatrix}, \quad \varphi_{j,k}^{(2)}(x, y) = \begin{pmatrix} 0 \\ \xi \end{pmatrix}, \\ \varphi_{j,k}^{(3)}(x, y) &= \begin{pmatrix} \eta \\ 0 \end{pmatrix}, \quad \varphi_{j,k}^{(4)}(x, y) = \begin{pmatrix} h_j^x \xi \\ -h_k^y \eta \end{pmatrix}, \quad \varphi_{j,k}^{(5)} = \begin{pmatrix} \eta^2 - 1/3 \\ 0 \end{pmatrix}, \\ \varphi_{j,k}^{(6)} &= \begin{pmatrix} 0 \\ \xi^2 - 1/3 \end{pmatrix}, \quad \varphi_{j,k}^{(7)} = \begin{pmatrix} h_j^x (\xi^2 - 1/3) \\ -2h_k^y \xi \eta \end{pmatrix}, \quad \varphi_{j,k}^{(8)} = \begin{pmatrix} -2h_j^x \xi \eta \\ h_k^y (\eta^2 - 1/3) \end{pmatrix}, \\ \varphi_{j,k}^{(9)} &= \begin{pmatrix} \eta^3 - \frac{3}{5}\eta \\ 0 \end{pmatrix}, \quad \varphi_{j,k}^{(10)} = \begin{pmatrix} 0 \\ \xi^3 - \frac{3}{5}\xi \end{pmatrix}, \quad \varphi_{j,k}^{(11)} = \begin{pmatrix} h_j^x (\xi^2 - 1/3)\eta \\ -h_k^y \xi (\eta^2 - 1/3) \end{pmatrix}, \\ \varphi_{j,k}^{(12)} &= \begin{pmatrix} h_j^x \xi (\eta^2 - 1/3) \\ -h_k^y (\eta^3 - \eta)/3 \end{pmatrix}, \quad \varphi_{j,k}^{(13)} = \begin{pmatrix} h_j^x (\xi^3 - \xi)/3 \\ -h_k^y (\xi^2 - 1/3)\eta \end{pmatrix}, \end{aligned}$$

where $\xi = 2(x - x_j)/h_j^x$, $\eta = 2(y - y_k)/h_k^y$, $h_j^x = x_{j+\frac{1}{2}} - x_{j-\frac{1}{2}}$, and $h_k^y = y_{k+\frac{1}{2}} - y_{k-\frac{1}{2}}$.

Multiplying Eq. (3.4) by the test function $\mathbf{w}(\mathbf{x}) \in \mathbf{W}^K(e_{j,k})$, integrating it over the cell $e_{j,k}$, and using the divergence theorem give

$$\frac{d}{dt} \int_{e_{j,k}} \mathbf{Q}(\mathbf{x}, t) \cdot \mathbf{w}(\mathbf{x}) \, d\mathbf{x} + \int_{\partial e_{j,k}} (\mathbf{F}_1^Q \cdot \mathbf{w}(\mathbf{x}) n_1 + \mathbf{F}_2^Q \cdot \mathbf{w}(\mathbf{x}) n_2) \, ds$$

$$= \int_{e_{j,k}} \mathbf{F}^Q \cdot \nabla \mathbf{w}(\mathbf{x}) \, d\mathbf{x}, \quad (3.5)$$

where $\mathbf{F}^Q = (\mathbf{F}_1^Q, \mathbf{F}_2^Q)^T$, and (n_1, n_2) denote the outer normal vector of cell boundary $\partial e_{j,k}$.

The approximate solution \mathbf{Q}_h may be expressed as follows

$$\mathbf{Q}_h(\mathbf{x}, t) = \sum_{\ell=0}^{D_W-1} Q_{j,k}^{(\ell)}(t) \boldsymbol{\varphi}_{j,k}^{(\ell)}(\mathbf{x}) =: \mathbf{Q}_{j,k}(\mathbf{x}, t), \quad \mathbf{x} \in e_{j,k}. \quad (3.6)$$

If the solution \mathbf{Q} in (3.5) and flux \mathbf{F}^Q on the cell boundary are replaced with the approximate solution \mathbf{Q}_h and numerical flux $\hat{\mathbf{F}}^Q$ (e.g. the Lax-Friedrichs flux), respectively, the test function is taken as the basis, and the integrals are evaluated by using the Gaussian quadrature, then the semi-discrete DG methods may be given as follows

$$\begin{aligned} & \sum_{m=0}^{D_W-1} \left(\int_{e_{j,k}} \boldsymbol{\varphi}_{j,k}^{(m)}(\mathbf{x}) \cdot \boldsymbol{\varphi}_{j,k}^{(\iota)}(\mathbf{x}) \, d\mathbf{x} \right) \frac{dQ_{j,k}^{(m)}(t)}{dt} \\ &= - |\partial e_{j,k}| \sum_{l=1}^{\tilde{q}} \omega_l \left(\hat{\mathbf{F}}_1^Q(\mathbf{U}(\tilde{\mathbf{x}}_l^G, t)) n_1 + \hat{\mathbf{F}}_2^Q(\mathbf{U}(\tilde{\mathbf{x}}_l^G, t)) n_2 \right) \cdot \boldsymbol{\varphi}_{j,k}^{(\iota)}(\tilde{\mathbf{x}}_l^G) \\ &+ |e_{j,k}| \sum_{\ell=1}^q \omega_\ell \mathbf{F}^Q(\mathbf{U}_{j,k}(\mathbf{x}_\ell^G, t)) \cdot \nabla \boldsymbol{\varphi}_{j,k}^{(\iota)}(\mathbf{x}_\ell^G), \quad \iota = 0, 1, \dots, D_W - 1, \end{aligned} \quad (3.7)$$

where $\mathbf{U}_{j,k} = (\mathbf{R}_{j,k}^T, \mathbf{Q}_{j,k}^T)^T$. The system (3.7) may be considered as a nonlinear system of ordinary differential equations with respect to the degree of freedom or moments $Q_{j,k}^{(m)}$, and approximated by using the explicit Runge-Kutta time discretization to give a fully-discrete locally divergence-free DG methods.

Remark 3.1 *The approximate magnetic field \mathbf{Q}_h obtained above is divergence free in each cell, but it is not continuous in general across the cell boundary. In view of this fact, such DG methods are called as locally divergence-free [30].*

3.2 Adaptive WENO limiter

The above DG methods may be directly used to solve the problem whose solution is smooth or only contains weak discontinuity, but the limiting procedure is needed to suppress the numerical oscillations in solving the problem containing the strong discontinuity. In solving the system (3.2), the limiting procedure used in the Runge-Kutta DG methods should ensure that the new approximate magnetic field does still satisfy the divergence-free constraint. This paper uses the WENO limiting procedure, whose implementation consists of two parts: identify the “troubled” cells and reconstruct the new approximate solution in the “troubled” cells.

Step I: identify “troubled” cells It is the same as the way used for the RHD equations in [66] by identifying the cell $e_{j,k}$ in the x and y directions, respectively. In each direction of the identification process, the modified TVB minmod function is applied to the characteristic variables in that direction, where the characteristic variables are calculated by using the eigenvectors corresponding to the system (3.2), for example, the characteristic variables in the x direction is calculated by $\mathbf{L}_1 \mathbf{U}$, here \mathbf{L}_1 denotes the left eigenvector matrix of the Jacobian matrix $\partial \mathbf{F}_1 / \partial \mathbf{U}$. If the cell $e_{j,k}$ is identified as a “troubled” cell in x or y direction then the cell $e_{j,k}$ is marked as $e_{j,k}^{tc}$, and go to **Step II**; otherwise the next cell is continuously checked.

Step II: reconstruct new approximate solution in “troubled” cell (i) Calculate the cell averages of characteristic variables, denoted by $\{\mathbf{W}_{i,\ell}^{(0)}\}$, use the WENO technique for the characteristic variables \mathbf{W} to reconstruct the new approximate values $\mathbf{W}_{m,p}^G$ of \mathbf{W} at the Gaussian points (x_m^G, y_p^G) in the “troubled” cell $e_{j,k}^{tc}$. After that, calculate the point value $\mathbf{U}_{m,p}^G$ of the conservative vector, and divide it into two parts $\mathbf{R}_{m,p}^G$ and $\mathbf{Q}_{m,p}^G$.

(ii) Derive the new approximate solutions $\mathbf{R}_{j,k}^{WENO}(x, y, t_n)$ and $\mathbf{Q}_{j,k}^{WENO}(x, y, t_n)$ by using the numerical integration and the approximate values of solution at the Gaussian points as follows

$$\mathbf{R}_{j,k}^{WENO}(x, y, t_n) := \mathbf{R}_{j,k}^{(0)} \phi_{j,k}^{(0)}(x, y) + \sum_{\ell=1}^{K(K+3)/2} \mathbf{R}_{j,k}^{(\ell), WENO} \phi_{j,k}^{(\ell)}(x, y), \quad (x, y) \in e_{j,k}^{tc},$$

where $\{\phi_{j,k}^{(\ell)}(x, y)\}$ are a set of basis functions of $\mathbb{P}^K(e_{j,k}^{tc})$, satisfying the orthogonal properties, and the higher order moments are given by the following formula

$$\begin{aligned} \mathbf{R}_{j,k}^{(\ell), WENO} &:= \frac{1}{a_\ell} \int_{e_{j,k}^{tc}} \mathbf{R}_{j,k}^{WENO}(x, y, t_n) \phi_{j,k}^{(\ell)}(x, y) \, dxdy \\ &\approx \frac{h_j^x h_k^y}{a_\ell} \sum_{m=1}^q \sum_{p=1}^q \omega_{m,p} \mathbf{R}_{m,p}^G \phi_{j,k}^{(\ell)}(x_m^G, y_p^G), \quad 1 \leq \ell \leq K(K+3)/2, \end{aligned}$$

where $a_\ell = \int_{e_{j,k}^{tc}} (\phi_{j,k}^{(\ell)}(x, y))^2 \, dxdy$, the new approximate magnetic field is given by

$$\begin{aligned} \mathbf{Q}_{j,k}^{WENO}(x, y, t_n) &= \mathbf{Q}_{j,k}^{(0)} \varphi_{j,k}^{(0)}(x, y) + \mathbf{Q}_{j,k}^{(1)} \varphi_{j,k}^{(1)}(x, y) \\ &\quad + \sum_{\ell=2}^{D_W-1} \mathbf{Q}_{j,k}^{(\ell), WENO} \varphi_{j,k}^{(\ell)}(x, y), \quad (x, y) \in e_{j,k}^{tc}, \end{aligned}$$

where higher-order moments $\mathbf{Q}_{j,k}^{(\ell), WENO}$, $l = 2, \dots, D_W - 1$, satisfy the following linear system

$$\begin{aligned} &\sum_{\ell=2}^{D_W-1} \left(\int_{e_{j,k}^{tc}} \varphi_{j,k}^{(\ell)}(x, y) \cdot \varphi_{j,k}^{(l)}(x, y) \, dxdy \right) \mathbf{Q}_{j,k}^{(\ell), WENO} \\ &= h_j^x h_k^y \sum_{m=1}^q \sum_{p=1}^q \omega_{m,p} \mathbf{Q}_{m,p}^G \cdot \varphi_{j,k}^{(l)}(x_m^G, y_p^G), \quad 2 \leq l \leq D_W - 1. \end{aligned}$$

After getting $\mathbf{R}_{j,k}^{WENO}(x, y, t_n)$ and $\mathbf{Q}_{j,k}^{WENO}(x, y, t_n)$, they are used to replace the original DG solutions in $e_{j,k}^{tc}$. Up to now the solution in the “troubled” cell $e_{j,k}^{tc}$ is modified. Go to **Step I** and check the next cell.

4 “Exactly” divergence-free DG methods

This section introduces the “exactly” divergence-free central DG methods for two-dimensional RMHD equations (3.2). Similar to the locally divergence-free DG methods proposed in Section 3, the conservative vector \mathbf{U} in the central DG methods is still written into two parts

$$\mathbf{R} = (D, m_x, m_y, m_z, B_z, E), \quad \mathbf{Q} = (B_x, B_y),$$

and apply the different spatial approximations to the governing equations for \mathbf{R} and \mathbf{Q} .

4.1 Spatial approximation

For the sake of convenience, we first give the central DG methods with the explicit Euler time discretization. Divide the computational domain Ω into two mutually dual meshes, denoted by $\{C_{j,k}\}$ and $\{D_{j+\frac{1}{2},k+\frac{1}{2}}\}$, respectively, where $C_{j,k} = (x_{j-\frac{1}{2}}, x_{j+\frac{1}{2}}) \times (y_{k-\frac{1}{2}}, y_{k+\frac{1}{2}})$, $D_{j+\frac{1}{2},k+\frac{1}{2}} = (x_j, x_{j+1}) \times (y_k, y_{k+1})$. The aim of central DG methods is to find two approximate solutions \mathbf{U}_h^C and \mathbf{U}_h^D , where corresponding DG approximations of \mathbf{R} is denoted by \mathbf{R}_h^C and \mathbf{R}_h^D , while \mathbf{Q}_h^C and \mathbf{Q}_h^D are used to denote corresponding DG approximations of \mathbf{Q} .

Because the divergence free constraint (3.1) is not considered in the equations (3.3) for \mathbf{R} , Eq. (3.3) may be directly discretized in the central DG framework, see [65], that is, we find two approximate solutions \mathbf{R}_h^C and \mathbf{R}_h^D such that their each component belongs to the following finite dimensional spaces

$$\begin{aligned} \mathcal{V}^C &:= \left\{ v(\mathbf{x}) \in L^1(\Omega) \mid v(\mathbf{x}) \in \mathbb{P}^K(C_{j,k}), \mathbf{x} \in C_{j,k} \subset \Omega, \forall j, k \right\}, \\ \mathcal{V}^D &:= \left\{ w(\mathbf{x}) \in L^1(\Omega) \mid w(\mathbf{x}) \in \mathbb{P}^K(D_{j+\frac{1}{2},k+\frac{1}{2}}), \mathbf{x} \in D_{j+\frac{1}{2},k+\frac{1}{2}} \subset \Omega, \forall j, k \right\}. \end{aligned}$$

If giving the DG solutions $\mathbf{U}_h^{C,n}$ and $\mathbf{U}_h^{D,n}$ at $t = t_n$, then the DG solution $\mathbf{R}_h^{C,n+1}$ at t_{n+1} satisfies

$$\begin{aligned} \int_{C_{j,k}} \mathbf{R}_h^{C,n+1} v(\mathbf{x}) d\mathbf{x} &= \int_{C_{j,k}} \left(\theta \mathbf{R}_h^{D,n} + (1 - \theta) \mathbf{R}_h^{C,n} \right) v(\mathbf{x}) d\mathbf{x} \\ &+ \Delta t_n \left(\int_{C_{j,k}} \mathbf{F}^R(\mathbf{U}_h^{D,n}) \cdot \nabla v(\mathbf{x}) d\mathbf{x} - \int_{\partial C_{j,k}} \mathbf{F}^R(\mathbf{U}_h^{D,n}) \cdot \mathbf{n} v(\mathbf{x}) ds \right), \quad \forall v(\mathbf{x}) \in \mathbb{P}^K(C_{j,k}), \end{aligned}$$

where $\Delta t_n = t_{n+1} - t_n$ denotes the practical time stepsize, $\theta = \Delta t_n / \tau_n$, and τ_n is the maximum timestep allowed by the CFL condition. Similarly, the approximate solution $\mathbf{R}_h^{D,n+1}$ on the mesh $\{D_{j+\frac{1}{2},k+\frac{1}{2}}\}$ satisfies the following equation

$$\begin{aligned} \int_{D_{j+\frac{1}{2},k+\frac{1}{2}}} \mathbf{R}_h^{D,n+1} w(\mathbf{x}) d\mathbf{x} &= \int_{D_{j+\frac{1}{2},k+\frac{1}{2}}} \left(\theta \mathbf{R}_h^{C,n} + (1 - \theta) \mathbf{R}_h^{D,n} \right) w(\mathbf{x}) d\mathbf{x} \\ &+ \Delta t_n \left(\int_{D_{j+\frac{1}{2},k+\frac{1}{2}}} \mathbf{F}^R(\mathbf{U}_h^{C,n}) \cdot \nabla w(\mathbf{x}) d\mathbf{x} - \int_{\partial D_{j+\frac{1}{2},k+\frac{1}{2}}} \mathbf{F}^R(\mathbf{U}_h^{C,n}) \cdot \mathbf{n} w(\mathbf{x}) ds \right), \end{aligned}$$

for all $w(\mathbf{x}) \in \mathbb{P}^K(D_{j+\frac{1}{2},k+\frac{1}{2}})$.

Due to the need to consider the divergence free constraint (3.1), the finite dimensional space for the approximation of \mathbf{Q} is different from that for \mathbf{R} , and is denoted as follows

$$\begin{aligned} \mathcal{M}^C &:= \{ \mathbf{v}(\mathbf{x}) \mid \nabla \cdot \mathbf{v} = 0, \mathbf{v}(\mathbf{x}) \in \mathcal{W}^K(C_{j,k}), \mathbf{x} \in C_{j,k}, \forall j, k \}, \\ \mathcal{M}^D &:= \{ \mathbf{w}(\mathbf{x}) \mid \nabla \cdot \mathbf{w} = 0, \mathbf{w}(\mathbf{x}) \in \mathcal{W}^K(D_{j+\frac{1}{2},k+\frac{1}{2}}), \mathbf{x} \in D_{j+\frac{1}{2},k+\frac{1}{2}}, \forall j, k \}, \end{aligned}$$

where

$$\mathcal{W}^K(\mathcal{T}) := [\mathbb{P}^K(\mathcal{T})]^2 \oplus \text{span}\{ \nabla \times (x^{K+1}y), \nabla \times (xy^{K+1}) \},$$

here \mathcal{T} denotes $C_{j,k}$ or $D_{j+\frac{1}{2},k+\frac{1}{2}}$, the symbol “ \oplus ” denotes the direct sum. The central DG methods for the \mathbf{Q} equations are to find the approximate solution $\mathbf{Q}_h^C \in \mathcal{M}^C$ and $\mathbf{Q}_h^D \in \mathcal{M}^D$ of \mathbf{Q} .

In the following, we provide how to get the approximate magnetic field $\mathbf{Q}_h^{C,n+1} = (B_{x,h}^{C,n+1}, B_{y,h}^{C,n+1})^T$ on the mesh $\{C_{j,k}\}$ at time t_{n+1} . It will consist of two steps: the approximate normal magnetic field is first gotten by solving the magnetic equation on the cell boundary, and then used to reconstruct the magnetic field in the cell. Take the cell $C_{j,k}$ as an example in the following.

Step (i) Find the approximate normal magnetic fields $b_{j\pm\frac{1}{2},k}^x(y)$ on the left and right boundaries $x = x_{j\pm\frac{1}{2}}$ of cell $C_{j,k}$, and $b_{j,k\pm\frac{1}{2}}^y(x)$ on the top and bottom boundaries $y = y_{k\pm\frac{1}{2}}$. Because B_x and B_y satisfy

$$\frac{\partial B_x}{\partial t} + \frac{\partial G}{\partial y} = 0, \quad (4.1)$$

$$\frac{\partial B_y}{\partial t} - \frac{\partial G}{\partial x} = 0, \quad (4.2)$$

where $G = G(\mathbf{U}) = B_x v_y - B_y v_x$, they may be solved by using the one-dimensional central DG methods, that is, find $b_{j-\frac{1}{2},k}^x(y) \in \mathbb{P}^K((y_{k-\frac{1}{2}}, y_{k+\frac{1}{2}}))$ satisfying

$$\int_{y_{k-\frac{1}{2}}}^{y_{k+\frac{1}{2}}} b_{j-\frac{1}{2},k}^x(y) \mu(y) dy = \int_{y_{k-\frac{1}{2}}}^{y_{k+\frac{1}{2}}} \left(\theta B_{x,h}^{D,n}(x_{j-\frac{1}{2}}, y) + (1 - \theta) B_{x,h}^{C,n}(x_{j-\frac{1}{2}}, y) \right) \mu(y) dy$$

$$+ \Delta t_n \left(\int_{y_{k-\frac{1}{2}}}^{y_{k+\frac{1}{2}}} G(U_h^{D,n}(x_{j-\frac{1}{2}}, y)) \frac{\partial \mu(y)}{\partial y} dy - G_{j-\frac{1}{2}, k+\frac{1}{2}}^{D,n} \mu(y_{k+\frac{1}{2}}) + G_{j-\frac{1}{2}, k-\frac{1}{2}}^{D,n} \mu(y_{k-\frac{1}{2}}) \right),$$

for any $\mu(y) \in \mathbb{P}^K((y_{k-\frac{1}{2}}, y_{k+\frac{1}{2}}))$, and find $b_{j, k-\frac{1}{2}}^y(x) \in \mathbb{P}^K((x_{j-\frac{1}{2}}, x_{j+\frac{1}{2}}))$ satisfying

$$\begin{aligned} \int_{x_{j-\frac{1}{2}}}^{x_{j+\frac{1}{2}}} b_{j, k-\frac{1}{2}}^y(x) \sigma(x) dx &= \int_{x_{j-\frac{1}{2}}}^{x_{j+\frac{1}{2}}} \left(\theta B_{y, h}^{D,n}(x, y_{k-\frac{1}{2}}) + (1 - \theta) B_{y, h}^{C,n}(x, y_{k-\frac{1}{2}}) \right) \sigma(x) dx \\ &+ \Delta t_n \left(\int_{x_{j-\frac{1}{2}}}^{x_{j+\frac{1}{2}}} -G(U_h^{D,n}(x, y_{k-\frac{1}{2}})) \frac{\partial \sigma(x)}{\partial x} dx + G_{j+\frac{1}{2}, k-\frac{1}{2}}^{D,n} \sigma(x_{j+\frac{1}{2}}) - G_{j-\frac{1}{2}, k-\frac{1}{2}}^{D,n} \sigma(x_{j-\frac{1}{2}}) \right), \end{aligned}$$

for any $\sigma(x) \in \mathbb{P}^K((x_{j-\frac{1}{2}}, x_{j+\frac{1}{2}}))$, where $G_{j-\frac{1}{2}, k+\frac{1}{2}}^{D,n} := G(U_h^{D,n}(x_{j-\frac{1}{2}}, y_{k+\frac{1}{2}}))$. The normal magnetic fields $b_{j+\frac{1}{2}, k}^x(y)$ and $b_{j, k+\frac{1}{2}}^y(x)$ may be solved by similar approach.

Step (ii) Reconstruct the magnetic field $\mathbf{Q}_h^{C, n+1}|_{C_{j,k}} = (B_{x,j,k}^{C, n+1}, B_{y,j,k}^{C, n+1})^T$ in the cell $C_{j,k}$, where $B_{x,j,k}^{C, n+1}, B_{y,j,k}^{C, n+1} \in \mathcal{W}^K(C_{j,k})$ and satisfy

$$\begin{aligned} B_{x,j,k}^{C, n+1}(x_{j+\frac{1}{2}}, y) &= b_{j+\frac{1}{2}, k}^x(y), \quad y \in (y_{k-\frac{1}{2}}, y_{k+\frac{1}{2}}), \\ B_{x,j,k}^{C, n+1}(x_{j-\frac{1}{2}}, y) &= b_{j-\frac{1}{2}, k}^x(y), \quad y \in (y_{k-\frac{1}{2}}, y_{k+\frac{1}{2}}), \\ B_{y,j,k}^{C, n+1}(x, y_{k+\frac{1}{2}}) &= b_{j, k+\frac{1}{2}}^y(x), \quad x \in (x_{j-\frac{1}{2}}, x_{j+\frac{1}{2}}), \\ B_{y,j,k}^{C, n+1}(x, y_{k-\frac{1}{2}}) &= b_{j, k-\frac{1}{2}}^y(x), \quad x \in (x_{j-\frac{1}{2}}, x_{j+\frac{1}{2}}), \end{aligned} \tag{4.3}$$

$$\frac{\partial B_{x,j,k}^{C, n+1}}{\partial x} + \frac{\partial B_{y,j,k}^{C, n+1}}{\partial y} = 0, \quad (x, y) \in C_{j,k}. \tag{4.4}$$

Before giving the detailed expressions of $B_{x,j,k}^{C, n+1}$ and $B_{y,j,k}^{C, n+1}$, a necessary condition is first discussed for the solution of the system of equations (4.3) and (4.4). If such the system exists the solution, then integrating (4.4) over the cell $C_{j,k}$ and using the divergence theorem and Eq. (4.3) gives

$$\int_{x_{j-\frac{1}{2}}}^{x_{j+\frac{1}{2}}} (b_{j, k-\frac{1}{2}}^y(x) - b_{j, k+\frac{1}{2}}^y(x)) dx + \int_{y_{k-\frac{1}{2}}}^{y_{k+\frac{1}{2}}} (b_{j-\frac{1}{2}, k}^x(y) - b_{j+\frac{1}{2}, k}^x(y)) dy = 0, \tag{4.5}$$

which is a necessary condition for the solution of the system of equations (4.3) and (4.4). It is proved in [32] that the normal magnetic field obtained by using the central DG methods satisfies (4.5).

The following provides the expressions of $B_{x,j,k}^{C, n+1}$ and $B_{y,j,k}^{C, n+1}$ for $K = 1, 2, 3$.

When $K = 1$, the normal magnetic fields on the cell boundary are

$$b_{j\pm\frac{1}{2}, k}^x(y) = b_{j\pm\frac{1}{2}, k}^{x, (0)} + b_{j\pm\frac{1}{2}, k}^{x, (1)} \eta,$$

$$b_{j,k\pm\frac{1}{2}}^y(x) = b_{j,k\pm\frac{1}{2}}^{y,(0)} + b_{j,k\pm\frac{1}{2}}^{y,(1)}\xi,$$

where $\xi = 2(x - x_j)/h_j^x$, $\eta = 2(y - y_k)/h_k^y$, and the reconstructed magnetic fields in the cell are

$$\begin{aligned} B_{x,j,k}^{C,n+1}(x, y) &= a_0 + a_1\xi + a_2\eta + a_3(\xi^2 - 1/3) + a_4\xi\eta, \\ B_{y,j,k}^{C,n+1}(x, y) &= b_0 + b_1\xi + b_2\eta + b_3\xi\eta + b_4(\eta^2 - 1/3), \end{aligned}$$

where the coefficients are given by

$$\begin{aligned} a_0 &= \frac{1}{2}(b_{j+\frac{1}{2},k}^{x,(0)} + b_{j-\frac{1}{2},k}^{x,(0)}) + \frac{h_j^x}{6h_k^y}(b_{j,k+\frac{1}{2}}^{y,(1)} - b_{j,k-\frac{1}{2}}^{y,(1)}), \\ b_0 &= \frac{1}{2}(b_{j,k+\frac{1}{2}}^{y,(0)} + b_{j,k-\frac{1}{2}}^{y,(0)}) + \frac{h_k^y}{6h_j^x}(b_{j+\frac{1}{2},k}^{x,(1)} - b_{j-\frac{1}{2},k}^{x,(1)}), \\ a_1 &= \frac{1}{2}(b_{j+\frac{1}{2},k}^{x,(0)} - b_{j-\frac{1}{2},k}^{x,(0)}), \quad b_2 = \frac{1}{2}(b_{j,k+\frac{1}{2}}^{y,(0)} - b_{j,k-\frac{1}{2}}^{y,(0)}), \\ a_2 &= \frac{1}{2}(b_{j+\frac{1}{2},k}^{x,(1)} + b_{j-\frac{1}{2},k}^{x,(1)}), \quad b_1 = \frac{1}{2}(b_{j,k+\frac{1}{2}}^{y,(1)} + b_{j,k-\frac{1}{2}}^{y,(1)}), \\ a_3 &= -\frac{h_j^x}{4h_k^y}(b_{j,k+\frac{1}{2}}^{y,(1)} - b_{j,k-\frac{1}{2}}^{y,(1)}), \quad b_4 = -\frac{h_k^y}{4h_j^x}(b_{j+\frac{1}{2},k}^{x,(1)} - b_{j-\frac{1}{2},k}^{x,(1)}), \\ a_4 &= \frac{1}{2}(b_{j+\frac{1}{2},k}^{x,(1)} - b_{j-\frac{1}{2},k}^{x,(1)}), \quad b_3 = \frac{1}{2}(b_{j,k+\frac{1}{2}}^{y,(1)} - b_{j,k-\frac{1}{2}}^{y,(1)}). \end{aligned} \tag{4.6}$$

When $K = 2$, the normal magnetic fields on the cell boundary are

$$\begin{aligned} b_{j\pm\frac{1}{2},k}^x(y) &= b_{j\pm\frac{1}{2},k}^{x,(0)} + b_{j\pm\frac{1}{2},k}^{x,(1)}\eta + b_{j\pm\frac{1}{2},k}^{x,(2)}(\eta^2 - \frac{1}{3}), \\ b_{j,k\pm\frac{1}{2}}^y(x) &= b_{j,k\pm\frac{1}{2}}^{y,(0)} + b_{j,k\pm\frac{1}{2}}^{y,(1)}\xi + b_{j,k\pm\frac{1}{2}}^{y,(2)}(\xi^2 - \frac{1}{3}), \end{aligned}$$

and the reconstructed magnetic fields in the cell are given by

$$\begin{aligned} B_{x,j,k}^{C,n+1}(x, y) &= a_0 + a_1\xi + a_2\eta + a_3(\xi^2 - 1/3) + a_4\xi\eta \\ &\quad + a_5(\eta^2 - 1/3) + a_6(\xi^3 - \frac{3}{5}\xi) + a_7\xi(\eta^2 - \frac{1}{3}), \\ B_{y,j,k}^{C,n+1}(x, y) &= b_0 + b_1\xi + b_2\eta + b_3(\xi^2 - 1/3) + b_4\xi\eta \\ &\quad + b_5(\eta^2 - 1/3) + b_6(\xi^2 - \frac{1}{3})\eta + b_7(\eta^3 - \frac{3}{5}\eta), \end{aligned}$$

where the coefficients are

$$\begin{aligned} a_0 &= \frac{1}{2}(b_{j+\frac{1}{2},k}^{x,(0)} + b_{j-\frac{1}{2},k}^{x,(0)}) + \frac{h_j^x}{6h_k^y}(b_{j,k+\frac{1}{2}}^{y,(1)} - b_{j,k-\frac{1}{2}}^{y,(1)}), \\ b_0 &= \frac{1}{2}(b_{j,k+\frac{1}{2}}^{y,(0)} + b_{j,k-\frac{1}{2}}^{y,(0)}) + \frac{h_k^y}{6h_j^x}(b_{j+\frac{1}{2},k}^{x,(1)} - b_{j-\frac{1}{2},k}^{x,(1)}), \\ a_1 &= \frac{1}{2}(b_{j+\frac{1}{2},k}^{x,(0)} - b_{j-\frac{1}{2},k}^{x,(0)}) + \frac{h_j^x}{15h_k^y}(b_{j,k+\frac{1}{2}}^{y,(2)} - b_{j,k-\frac{1}{2}}^{y,(2)}), \end{aligned}$$

$$\begin{aligned}
b_2 &= \frac{1}{2}(b_{j,k+\frac{1}{2}}^{y,(0)} - b_{j,k-\frac{1}{2}}^{y,(0)}) + \frac{h_k^y}{15h_j^x}(b_{j+\frac{1}{2},k}^{x,(2)} - b_{j-\frac{1}{2},k}^{x,(2)}), \\
a_2 &= \frac{1}{2}(b_{j+\frac{1}{2},k}^{x,(1)} + b_{j-\frac{1}{2},k}^{x,(1)}), \quad a_4 = \frac{1}{2}(b_{j+\frac{1}{2},k}^{x,(1)} - b_{j-\frac{1}{2},k}^{x,(1)}), \\
b_1 &= \frac{1}{2}(b_{j,k+\frac{1}{2}}^{y,(1)} + b_{j,k-\frac{1}{2}}^{y,(1)}), \quad b_4 = \frac{1}{2}(b_{j,k+\frac{1}{2}}^{y,(1)} - b_{j,k-\frac{1}{2}}^{y,(1)}), \\
a_5 &= \frac{1}{2}(b_{j+\frac{1}{2},k}^{x,(2)} + b_{j-\frac{1}{2},k}^{x,(2)}), \quad a_7 = \frac{1}{2}(b_{j+\frac{1}{2},k}^{x,(2)} - b_{j-\frac{1}{2},k}^{x,(2)}), \\
b_3 &= \frac{1}{2}(b_{j,k+\frac{1}{2}}^{y,(2)} + b_{j,k-\frac{1}{2}}^{y,(2)}), \quad b_6 = \frac{1}{2}(b_{j,k+\frac{1}{2}}^{y,(2)} - b_{j,k-\frac{1}{2}}^{y,(2)}), \\
a_3 &= -\frac{h_j^x}{4h_k^y}(b_{j,k+\frac{1}{2}}^{y,(1)} - b_{j,k-\frac{1}{2}}^{y,(1)}), \quad a_6 = -\frac{h_j^x}{6h_k^y}(b_{j,k+\frac{1}{2}}^{y,(2)} - b_{j,k-\frac{1}{2}}^{y,(2)}), \\
b_5 &= -\frac{h_k^y}{4h_j^x}(b_{j+\frac{1}{2},k}^{x,(1)} - b_{j-\frac{1}{2},k}^{x,(1)}), \quad b_7 = -\frac{h_k^y}{6h_j^x}(b_{j+\frac{1}{2},k}^{x,(2)} - b_{j-\frac{1}{2},k}^{x,(2)}).
\end{aligned}$$

When $K = 3$, because the normal magnetic fields on the cell boundary are given by

$$\begin{aligned}
b_{j\pm\frac{1}{2},k}^x(y) &= b_{j\pm\frac{1}{2},k}^{x,(0)} + b_{j\pm\frac{1}{2},k}^{x,(1)}\eta + b_{j\pm\frac{1}{2},k}^{x,(2)}(\eta^2 - \frac{1}{3}) + b_{j\pm\frac{1}{2},k}^{x,(3)}(\eta^3 - \frac{3}{5}\eta), \\
b_{j,k\pm\frac{1}{2}}^y(x) &= b_{j,k\pm\frac{1}{2}}^{y,(0)} + b_{j,k\pm\frac{1}{2}}^{y,(1)}\xi + b_{j,k\pm\frac{1}{2}}^{y,(2)}(\xi^2 - \frac{1}{3}) + b_{j,k\pm\frac{1}{2}}^{y,(3)}(\xi^3 - \frac{3}{5}\xi),
\end{aligned}$$

the reconstructed magnetic fields in the cell are

$$\begin{aligned}
B_{x,j,k}^{C,n+1}(x,y) &= a_0 + a_1\xi + a_2\eta + a_3(\xi^2 - \frac{1}{3}) + a_4\xi\eta + a_5(\eta^2 - \frac{1}{3}) \\
&\quad + a_6(\xi^3 - \frac{3}{5}\xi) + a_7(\xi^2 - \frac{1}{3})\eta + a_8\xi(\eta^2 - \frac{1}{3}) \\
&\quad + a_9(\eta^3 - \frac{3}{5}\eta) + a_{10}(\xi^4 - \frac{6}{7}\xi^2 + \frac{3}{35}) + a_{11}\xi(\eta^3 - \frac{3}{5}\eta), \\
B_{y,j,k}^{C,n+1}(x,y) &= b_0 + b_1\xi + b_2\eta + b_3(\xi^2 - \frac{1}{3}) + b_4\xi\eta + b_5(\eta^2 - \frac{1}{3}) \\
&\quad + b_6(\xi^3 - \frac{3}{5}\xi) + b_7(\xi^2 - \frac{1}{3})\eta + b_8\xi(\eta^2 - \frac{1}{3}) \\
&\quad + b_9(\eta^3 - \frac{3}{5}\eta) + b_{10}\eta(\xi^3 - \frac{3}{5}\xi) + b_{11}(\eta^4 - \frac{6}{7}\eta^2 + \frac{3}{35}).
\end{aligned}$$

Some coefficients may be determined as follows

$$\begin{aligned}
a_0 &= \frac{1}{2}(b_{j+\frac{1}{2},k}^{x,(0)} + b_{j-\frac{1}{2},k}^{x,(0)}) + \frac{h_j^x}{6h_k^y}(b_{j,k+\frac{1}{2}}^{y,(1)} - b_{j,k-\frac{1}{2}}^{y,(1)}), \\
b_0 &= \frac{1}{2}(b_{j,k+\frac{1}{2}}^{y,(0)} + b_{j,k-\frac{1}{2}}^{y,(0)}) + \frac{h_k^y}{6h_j^x}(b_{j+\frac{1}{2},k}^{x,(1)} - b_{j-\frac{1}{2},k}^{x,(1)}), \\
a_1 &= \frac{1}{2}(b_{j+\frac{1}{2},k}^{x,(0)} - b_{j-\frac{1}{2},k}^{x,(0)}) + \frac{h_j^x}{15h_k^y}(b_{j,k+\frac{1}{2}}^{y,(2)} - b_{j,k-\frac{1}{2}}^{y,(2)}), \\
b_2 &= \frac{1}{2}(b_{j,k+\frac{1}{2}}^{y,(0)} - b_{j,k-\frac{1}{2}}^{y,(0)}) + \frac{h_k^y}{15h_j^x}(b_{j+\frac{1}{2},k}^{x,(2)} - b_{j-\frac{1}{2},k}^{x,(2)}),
\end{aligned}$$

$$\begin{aligned}
a_3 &= \frac{h_j^x}{h_k^y} \left(\frac{3}{70} (b_{j,k+\frac{1}{2}}^{y,(3)} - b_{j,k-\frac{1}{2}}^{y,(3)}) - \frac{1}{4} (b_{j,k+\frac{1}{2}}^{y,(1)} - b_{j,k-\frac{1}{2}}^{y,(1)}) \right), \\
b_5 &= \frac{h_k^y}{h_j^x} \left(\frac{3}{70} (b_{j+\frac{1}{2},k}^{x,(3)} - b_{j-\frac{1}{2},k}^{x,(3)}) - \frac{1}{4} (b_{j+\frac{1}{2},k}^{x,(1)} - b_{j-\frac{1}{2},k}^{x,(1)}) \right), \\
a_4 &= \frac{1}{2} (b_{j+\frac{1}{2},k}^{x,(1)} - b_{j-\frac{1}{2},k}^{x,(1)}), \quad b_4 = \frac{1}{2} (b_{j,k+\frac{1}{2}}^{y,(1)} - b_{j,k-\frac{1}{2}}^{y,(1)}), \\
a_5 &= \frac{1}{2} (b_{j+\frac{1}{2},k}^{x,(2)} + b_{j-\frac{1}{2},k}^{x,(2)}), \quad a_8 = \frac{1}{2} (b_{j+\frac{1}{2},k}^{x,(2)} - b_{j-\frac{1}{2},k}^{x,(2)}), \\
b_3 &= \frac{1}{2} (b_{j,k+\frac{1}{2}}^{y,(2)} + b_{j,k-\frac{1}{2}}^{y,(2)}), \quad b_7 = \frac{1}{2} (b_{j,k+\frac{1}{2}}^{y,(2)} - b_{j,k-\frac{1}{2}}^{y,(2)}), \\
a_6 &= -\frac{h_j^x}{6h_k^y} (b_{j,k+\frac{1}{2}}^{y,(2)} - b_{j,k-\frac{1}{2}}^{y,(2)}), \quad a_{10} = -\frac{h_j^x}{8h_k^y} (b_{j,k+\frac{1}{2}}^{y,(3)} - b_{j,k-\frac{1}{2}}^{y,(3)}), \\
b_9 &= -\frac{h_k^y}{6h_j^x} (b_{j+\frac{1}{2},k}^{x,(2)} - b_{j-\frac{1}{2},k}^{x,(2)}), \quad b_{11} = -\frac{h_k^y}{8h_j^x} (b_{j+\frac{1}{2},k}^{x,(3)} - b_{j-\frac{1}{2},k}^{x,(3)}), \\
a_9 &= \frac{1}{2} (b_{j+\frac{1}{2},k}^{x,(3)} + b_{j-\frac{1}{2},k}^{x,(3)}), \quad a_{11} = \frac{1}{2} (b_{j+\frac{1}{2},k}^{x,(3)} - b_{j-\frac{1}{2},k}^{x,(3)}), \\
b_6 &= \frac{1}{2} (b_{j,k+\frac{1}{2}}^{y,(3)} + b_{j,k-\frac{1}{2}}^{y,(3)}), \quad b_{10} = \frac{1}{2} (b_{j,k+\frac{1}{2}}^{y,(3)} - b_{j,k-\frac{1}{2}}^{y,(3)}),
\end{aligned}$$

while other four coefficients satisfy the following relations

$$a_2 + \frac{2}{3}a_7 = \frac{1}{2}(b_{j+\frac{1}{2},k}^{x,(1)} + b_{j-\frac{1}{2},k}^{x,(1)}), \quad b_1 + \frac{2}{3}b_8 = \frac{1}{2}(b_{j,k+\frac{1}{2}}^{y,(1)} + b_{j,k-\frac{1}{2}}^{y,(1)}), \quad h_y^k a_7 + h_j^x b_8 = 0. \quad (4.7)$$

The coefficients a_2 , a_7 , b_1 , and b_8 cannot be uniquely determined by (4.3) and (4.4). In order to uniquely determine them, an additional condition is needed. In our computations, the coefficient a_7 at t_{n+1} is obtained by solving Eq. (4.1) with the central DG methods, i.e.

$$\begin{aligned}
\int_{C_{j,k}} B_{x,h}^{C,n+1} v(\mathbf{x}) d\mathbf{x} &= \int_{C_{j,k}} (\theta B_{x,h}^{D,n} + (1-\theta) B_{x,h}^{C,n}) v(\mathbf{x}) d\mathbf{x} \\
&+ \Delta t_n \left(\int_{C_{j,k}} G(\mathbf{U}_h^{D,n}) \frac{\partial v(\mathbf{x})}{\partial y} d\mathbf{x} - \int_{\partial C_{j,k}} G(\mathbf{U}_h^{D,n}) n_2 v(\mathbf{x}) ds \right),
\end{aligned}$$

where $v(\mathbf{x})$ is taken as the basis function $(\xi^2 - 1/3)\eta$ corresponding to a_7 . After a_7 is gotten, the coefficients a_2 , b_8 , and b_1 may be calculated according to (4.7). Combining $\mathbf{R}_h^{C,n+1}$ with the approximate magnetic fields $\mathbf{Q}_h^{C,n+1}$ on the mesh $\{C_{j,k}\}$ at t_{n+1} derived by the above approach gives the fully approximate conservative vector $\mathbf{U}_h^{C,n+1}$. The approximate solution vector $\mathbf{U}_h^{D,n+1}$ may be similarly obtained, but is no longer repeated here.

The time discretization in the above central DG methods is only first-order accurate, the higher-order accurate explicit Runge-Kutta methods may be used to replace the forward Euler time discretization and improve the accuracy of central DG methods in time.

Remark 4.1 *Because the normal magnetic fields obtained by the above central DG methods are continuous across the cell boundary, the above central DG methods are “exactly” divergence-free [32].*

Remark 4.2 *The above methods need to calculate the flux at the corner of the rectangular cell when the approximate normal magnetic field is solved on the cell boundary. Naturally, the solutions on the dual mesh may be used.*

4.2 Adaptive WENO limiter

The limiting procedure is also needed for the “exactly” divergence-free central DG methods when they are used to solve the RMHD problems with strong discontinuity. The WENO limiting procedure is still independently applied to \mathbf{R}_h and \mathbf{Q}_h . Especially, the limiting procedure for the approximate solutions \mathbf{R}_h^C and \mathbf{R}_h^D is the same as that in the locally divergence-free DG methods, see Section 3.2, only but one needs to respectively identify the “troubled” cells in two mutually dual meshes and reconstruct new WENO approximate solutions replace \mathbf{R}_h^C and \mathbf{R}_h^D defined in the “troubled” cells, It will not be repeated here.

The above WENO limiting procedure cannot be directly applied to \mathbf{Q}_h , otherwise the normal component of limited magnetic field may be discontinuous across the cell boundary. In view of that \mathbf{Q}_h is derived by the reconstruction based on $b^x(y)$ and $b^y(x)$, a natural consideration is that the WENO limiting procedure is first applied to $b^x(y)$ and $b^y(x)$, then the limited magnetic field b^x and b^y are used to reconstruct the new magnetic field within the cell.

Take $b_{j-\frac{1}{2},k}^x(y)$ as an example to introduce the limiting procedure for the magnetic field. In fact it is the same as that used for the one-dimensional DG methods. For the sake of convenience, use $\mathcal{I}_{j-\frac{1}{2},k}$ to denote the boundary of cell $C_{j,k}$: $x = x_{j-\frac{1}{2}}, y_{k-\frac{1}{2}} \leq y \leq y_{k+\frac{1}{2}}$.

Step I : Use the modified TVB minmod function to check whether the normal magnetic field $b_{j-\frac{1}{2},k}^x(y)$ on the cell boundary $\mathcal{I}_{j-\frac{1}{2},k}$ is needed to be limited. Calculate

$$\tilde{b}_k^x := b_{j-\frac{1}{2},k}^x(y_{k+\frac{1}{2}}) - b_{j-\frac{1}{2},k}^{x,(0)}, \quad \tilde{\tilde{b}}_k^x := -b_{j-\frac{1}{2},k}^x(y_{k-\frac{1}{2}}) + b_{j-\frac{1}{2},k}^{x,(0)},$$

then apply the modified TVB minmod function to \tilde{b}_k^x and $\tilde{\tilde{b}}_k^x$

$$\tilde{b}_k^{x,mod} := \tilde{m}(\tilde{b}_k^x, \Delta_+ b_k^{x,(0)}, \Delta_- b_k^{x,(0)}), \quad \tilde{\tilde{b}}_k^{x,mod} := \tilde{m}(\tilde{\tilde{b}}_k^x, \Delta_+ b_k^{x,(0)}, \Delta_- b_k^{x,(0)}),$$

where

$$\Delta_+ b_k^{x,(0)} := b_{j-\frac{1}{2},k+1}^{x,(0)} - b_{j-\frac{1}{2},k}^{x,(0)}, \quad \Delta_- b_k^{x,(0)} := b_{j-\frac{1}{2},k}^{x,(0)} - b_{j-\frac{1}{2},k-1}^{x,(0)}.$$

If $\tilde{b}_k^{x,mod}$ is different from \tilde{b}_k^x , or $\tilde{b}_k^{x,mod}$ is different from \tilde{b}_k^x , then mark $\mathcal{I}_{j-\frac{1}{2},k}$ as “troubled” cell boundary, and go to **Step II**; otherwise check the approximate normal magnetic field on the next cell boundary.

Step II : Use the WENO technique to reconstruct the new normal magnetic field on “troubled” cell boundary $\mathcal{I}_{j-\frac{1}{2},k}$. Using the cell averages $\{b^{x,(0)}\}$ of $b^x(y)$ on the neighboring cell boundary of $\mathcal{I}_{j-\frac{1}{2},k}$ in the y direction and $2K+1$ order WENO reconstruction to get $b_m^{x,G}$, the new approximation of b^x at the Gaussian points y_m^G within the interval $(y_{k-\frac{1}{2}}, y_{k+\frac{1}{2}})$, where $m = 1, \dots, K+1$, then use numerical integration to give a new approximation of $b^x(y)$, for example, the new approximate solution for $K = 2$ is given by

$$b_{j-\frac{1}{2},k}^{x,WENO}(y) = b_{j-\frac{1}{2},k}^{x,(0)} + b_{j-\frac{1}{2},k}^{x,WENO,(1)} \phi_k^{(1)}(y) + b_{j-\frac{1}{2},k}^{x,WENO,(2)} \phi_k^{(2)}(y),$$

where $\phi_k^{(1)}(y) = \eta$, $\phi_k^{(2)}(y) = \eta^2 - 1/3$, and $\eta = 2(y - y_k)/h_k^y$, higher order moments may be determined by

$$b_{j-\frac{1}{2},k}^{x,WENO,(i)} \int_{y_{k-\frac{1}{2}}}^{y_{k+\frac{1}{2}}} \phi_k^{(i)}(y) \phi_k^{(i)}(y) dy = h_k^y \sum_{m=1}^{K+1} b_m^{x,G} w_m^G \phi_k^{(i)}(y_m^G), \quad i = 1, \dots, K,$$

where w_m^G is weight corresponding to the point y_m^G . Use the new normal magnetic field $b_{j-\frac{1}{2},k}^{x,WENO}(y)$ to replace the old normal magnetic field on $\mathcal{I}_{j-\frac{1}{2},k}$, and go to **Step I**.

Remark 4.3 *It is not difficult to know that the above WENO limiting procedure does not change the cell average value of magnetic field over the cell boundary so that the new normal magnetic field satisfies the necessary condition (4.5).*

5 Numerical Results

This section uses our P^K -based locally and “exactly” divergence-free Runge-Kutta DG methods with WENO limiter to solve several initial value problems or initial-boundary-value problems of one- and two-dimensional RMHD equations in order to demonstrate the accuracy and effectiveness of our Runge-Kutta DG methods. Because two solutions of “exactly” divergence-free central Runge-Kutta DG methods on mutually dual meshes are almost identical each other, only one of the central DG solutions will be shown in the following.

5.1 1D examples

This section will solve a smooth problem and three Riemann problems by the proposed DG methods. Unless otherwise stated, the third-order accurate explicit TVD Runge-Kutta method is used for the time discretization, see [65,66], the CFL numbers of P^1 -, P^2 -, P^3 -based non-central DG methods are taken as 0.3, 0.2, and 0.1, respectively, while the CFL numbers of P^1 -, P^2 -, P^3 -based central DG methods are chosen as 0.4, 0.3, and 0.2, respectively, and $\theta = 1$. The determination of time stepsize may be found in [65], and the parameter M in the modified TVB minmod function is taken as 500.

Example 5.1 (Smooth problem) This problem describes the periodic propagation of a sine wave within the domain $\Omega = [0, 1]$ and is used to test the accuracy of non-central and central DG methods. The detailed initial data are

$$\begin{aligned}\rho(x, 0) &= 1, \quad v_x(x, 0) = 0, \quad v_y(x, 0) = 0.1 \sin(2\pi x), \\ v_z(x, 0) &= 0.1 \cos(2\pi x), \quad B_x(x, 0) = 1, \quad B_y(x, 0) = \kappa v_y(x, 0), \\ B_z(x, 0) &= \kappa v_z(x, 0), \quad p(x, 0) = 0.1,\end{aligned}$$

where $\kappa = \sqrt{1 + \rho h \gamma^2}$, and corresponding exact solutions are

$$\begin{aligned}\rho(x, t) &= 1, \quad v_x(x, t) = 0, \quad v_y(x, t) = 0.1 \sin(2\pi(x + t/\kappa)), \\ v_z(x, t) &= 0.1 \cos(2\pi(x + t/\kappa)), \quad B_x(x, t) = 1, \quad B_y(x, t) = \kappa v_y(x, t), \\ B_z(x, t) &= \kappa v_z(x, t), \quad p(x, t) = 0.1.\end{aligned}$$

In our computations, the adiabatic index $\Gamma = 5/3$, the computational domain Ω is divided into N uniform cells and the periodic conditions are specified, and the fourth-order Runge-Kutta method mentioned in [66] is used in order to ensure the accuracy in time. Table 5.1 shows the l^1 errors in B_y and orders at $t = 1$ obtained by using the non-central and central DG methods without or with WENO limiter in global. It is seen that both non-central and central DG methods may get the theoretical orders, and the WENO limiter may not destroy the accuracy of DG methods.

What follows is that the non-central and central DG methods are used to solve three Riemann problems of 1D RMHD equations, whose exact solution are obtained by using the approach provided in [21].

Example 5.2 (Riemann problem 1) The initial data of the first Riemann problem are

$$(\rho, v_x, v_y, v_z, B_x, B_y, B_z, p) = \begin{cases} (1, 0, 0, 0, 0.5, 1, 0, 1), & x < 0, \\ (0.125, 0, 0, 0, 0.5, -1, 0, 0.1), & x > 0, \end{cases}$$

with the adiabatic index $\Gamma = 2$. It is an extension of Brio-Wu shock tube problem [10] in the non-relativistic MHDs. Its solution consists of a left-moving fast rarefaction

Table 5.1

l^1 errors in B_y and orders at $t = 1$ obtained by the non-central and central DG methods. The fourth-order accurate Runge-Kutta method and $N \times 2N$ uniform cells are used.

	N	without limiter				with limiter in global			
		non-central DG		central DG		non-central DG		central DG	
		l^1 error	order	l^1 error	order	l^1 error	order	l^1 error	order
P^1	10	1.15e-03	—	9.21e-04	—	9.94e-03	—	2.42e-03	—
	20	2.99e-04	1.94	2.40e-04	1.94	2.28e-03	2.12	4.82e-04	2.33
	40	7.56e-05	1.98	6.05e-05	1.99	5.52e-04	2.05	1.12e-04	2.11
	80	1.89e-05	2.00	1.52e-05	2.00	1.37e-04	2.02	2.74e-05	2.03
	160	4.74e-06	2.00	3.79e-06	2.00	3.40e-05	2.01	6.81e-06	2.01
	320	1.19e-06	2.00	9.48e-07	2.00	8.49e-06	2.00	1.70e-06	2.00
P^2	10	5.73e-05	—	2.93e-05	—	2.61e-03	—	1.20e-03	—
	20	7.21e-06	2.99	3.83e-06	2.94	4.41e-05	5.88	4.68e-05	4.68
	40	9.09e-07	2.99	4.83e-07	2.98	5.47e-06	3.01	1.99e-06	4.55
	80	1.14e-07	2.99	6.06e-08	3.00	1.01e-06	2.43	1.31e-07	3.92
	160	1.43e-08	2.99	7.59e-09	3.00	1.37e-07	2.89	1.29e-08	3.35
	320	1.80e-09	3.00	9.49e-10	3.00	1.75e-08	2.97	1.50e-09	3.10
P^3	10	2.40e-06	—	1.28e-06	—	5.91e-05	—	3.43e-05	—
	20	1.53e-07	3.97	7.96e-08	4.01	7.89e-07	6.23	4.77e-07	6.17
	40	9.53e-09	4.01	5.01e-09	3.99	8.16e-08	3.28	1.74e-08	4.78
	80	5.96e-10	4.00	3.13e-10	4.00	5.77e-09	3.82	9.44e-10	4.20
	160	3.73e-11	4.00	1.96e-11	4.00	3.71e-10	3.96	5.69e-11	4.05
	320	2.33e-12	4.00	1.22e-12	4.00	2.33e-11	3.99	3.51e-12	4.02

wave, a slow compound wave, a contact discontinuity, a right-moving slow shock wave, and a right-moving fast rarefaction wave. There is an argument about the validity of the compound wave, which exists in the numerical results given by any shock capturing scheme, but does not appear in the exact solution obtained by the analytical calculation [63].

Figs. 5.1, 5.2, and 5.3 plot the densities ρ , Lorentz factors γ , and magnetic fields B_y at $t = 0.4$ obtained by using the non-central and central DG methods. It is seen that those numerical solutions are in good agreement with the exact solutions, there exist more obvious numerical oscillations at the left-hand side of the compound wave in the solutions obtained by the P^3 -based non-central DG methods, but the numerical

oscillation is not too obvious in the solution of the central DG methods. Moreover, the non-central DG methods identify more “troubled” cells than the central DG, see Fig. 5.4.

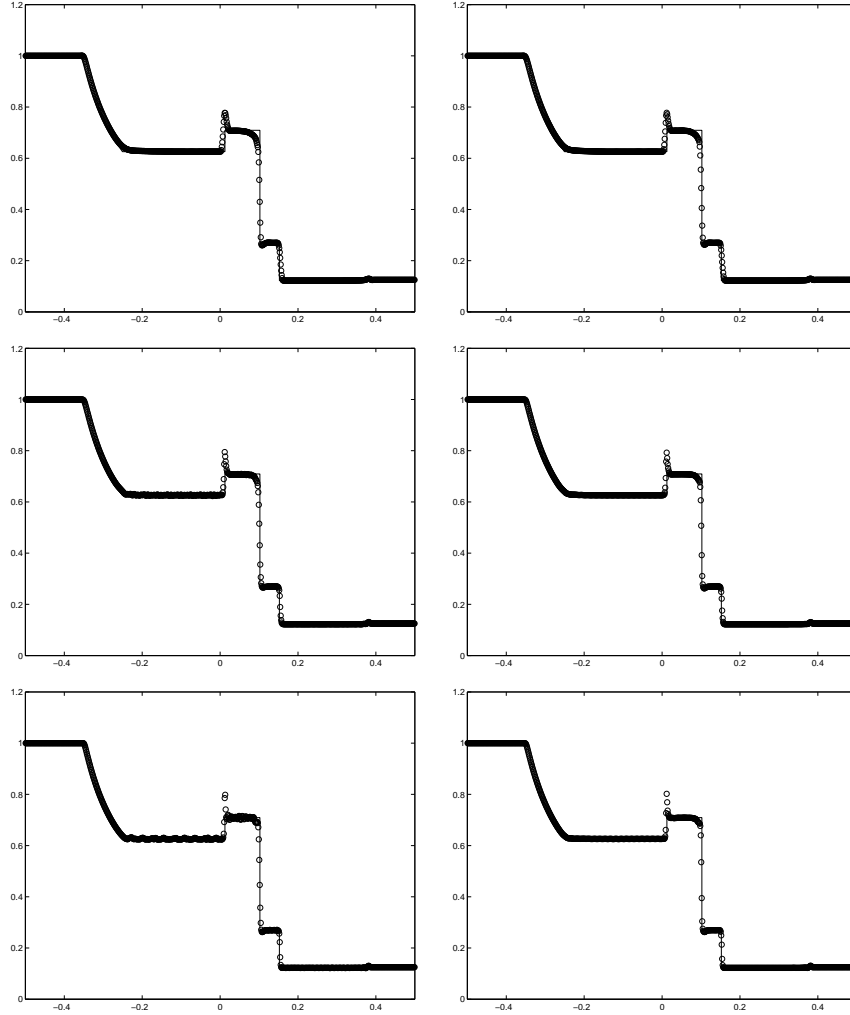


Figure 5.1. Example 5.2 The densities ρ at $t = 0.4$. The solid line denotes the exact solution, while the symbol “o” is numerical solution obtained with 800 cells. Left: P^K -based non-central DG methods; right: P^K -based central DG methods. From top to bottom: $K = 1, 2, 3$.

Example 5.3 (Riemann problem 2) The initial data of second Riemann problem are

$$(\rho, v_x, v_y, v_z, B_x, B_y, B_z, p) = \begin{cases} (1, 0, 0, 0, 5, 6, 6, 30), & x < 0, \\ (1, 0, 0, 0, 5, 0.7, 0.7, 1), & x > 0, \end{cases}$$

with the adiabatic index $\Gamma = 5/3$. As time increases, the initial discontinuity will decompose into two left-moving rarefaction waves, and a contact discontinuity and two right-moving shock waves.

Figs 5.5, 5.6, and 5.7 display the densities ρ , velocities v_y , and magnetic fields B_y at $t = 0.4$. It can be seen from the plots that high order methods resolves the contact

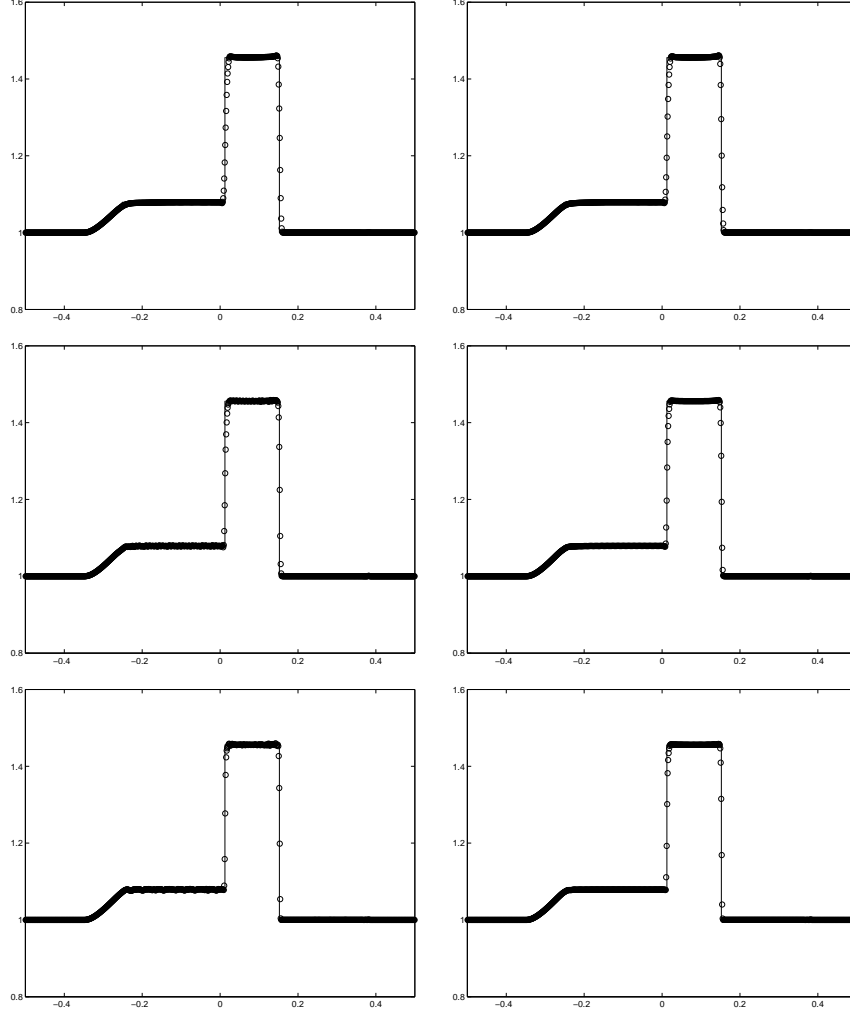


Figure 5.2. Same as Fig. 5.1 except for the Lorentz factor γ .

discontinuity in the density and two right-moving shock waves better than the lower order method, and the non-central and central DG methods have essentially the same resolution. The “troubled” cells identified by the present DG methods are very finite, and mainly appear in the region where the discontinuities in solution are relatively strong, see Fig. 5.8.

Example 5.4 (Riemann problem 3) The initial data of last 1D Riemann problem are taken as

$$(\rho, v_x, v_y, v_z, B_x, B_y, B_z, p) = \begin{cases} (1, 0, 0, 0, 10, 7, 7, 1000), & x < 0, \\ (1, 0, 0, 0, 10, 0.7, 0.7, 0.1), & x > 0, \end{cases}$$

with the adiabatic index $\Gamma = 5/3$. It has the same wave structure as Example 5.3, but two right-moving shock waves are very strong due to high ratio of initial pressures, and their speeds are very close to that of contact discontinuity so that the difficulty of numerical simulation is seriously increased.

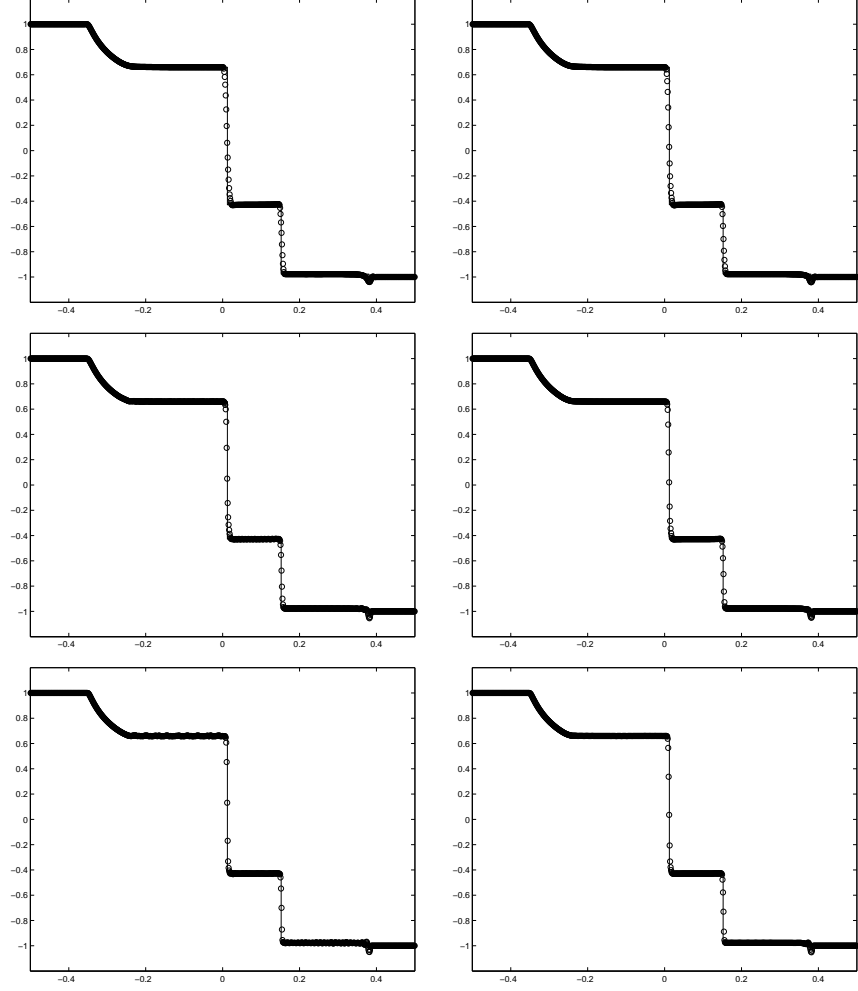


Figure 5.3. Same as Fig. 5.1 except for B_y .

Figs. 5.9, 5.10, and 5.11 give the densities ρ , the velocities v_y , and magnetic fields B_y at $t = 0.4$ obtained by using the non-central and central DG methods. The results show that the densities ρ and velocities v_y of P^3 -based DG methods are obviously better than those of the P^1 - and P^2 -based DG methods. There is no obvious difference between the non-central and central methods of the same order, and the numbers of “troubled” cells is also basically the same, see Fig. 5.12.

5.2 2D examples

This section will solve a smooth problem, Orszag-Tang problem, blast problem, Rotor problem, and the interaction between the shock wave and cloud by the proposed DG methods. Unless otherwise stated, the determination of time stepsize is the same as the above and the parameter M in the modified TVB minmod function is taken as 50.

Example 5.5 (Smooth problem) It describes the periodic propagation of a sine

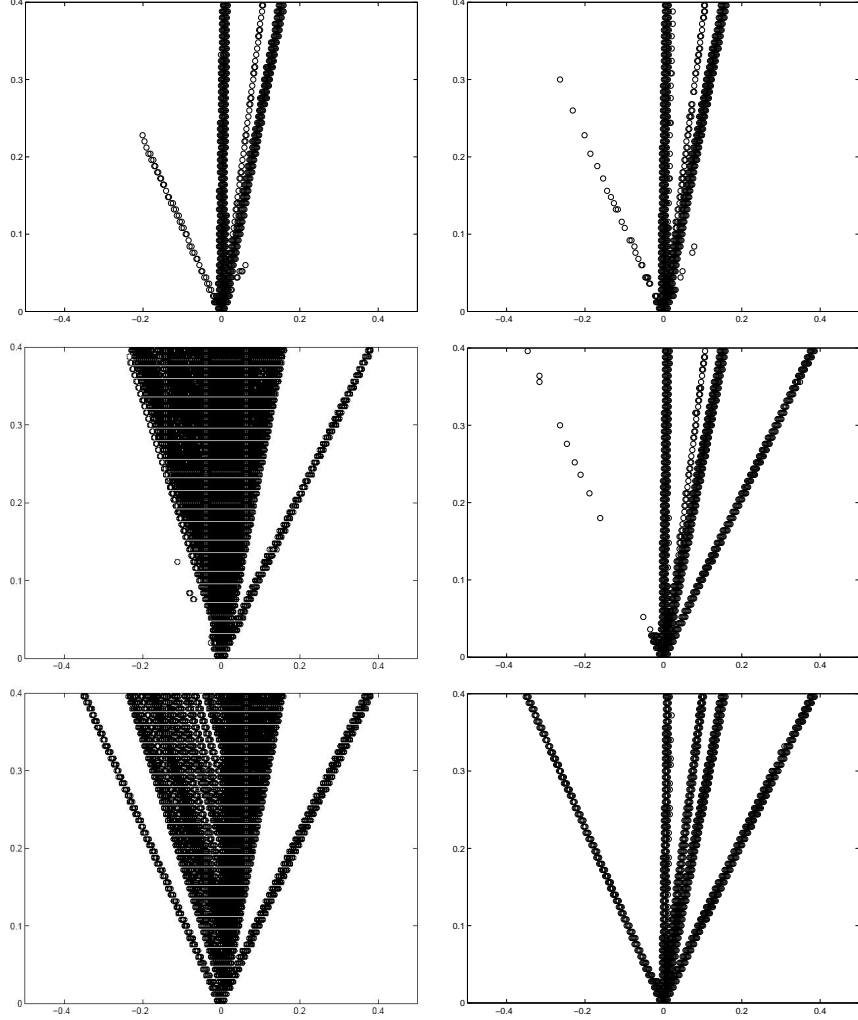


Figure 5.4. Example 5.2: The time evolution of “troubled” cells. Left: non-central DG methods; right: central DG methods. From top to bottom: $K = 1, 2, 3$. The cell number is 800.

wave within the domain $[0, 2/\sqrt{3}] \times [0, 2]$ and is used to test the accuracy of proposed DG methods. The angle between the direction of propagation and the x -axis is $\alpha = 30^\circ$. The detailed initial conditions are

$$\begin{aligned} \rho(x, y, 0) &= 1, \quad v_x(x, y, 0) = -0.1 \sin(2\pi\zeta) \sin \alpha, \\ v_y(x, y, 0) &= 0.1 \sin(2\pi\zeta) \cos \alpha, \quad v_z(x, y, 0) = 0.1 \cos(2\pi\zeta), \\ B_x(x, y, 0) &= \cos \alpha + \kappa v_x(x, y, 0), \quad B_y(x, y, 0) = \sin \alpha + \kappa v_y(x, y, 0), \\ B_z(x, y, 0) &= \kappa v_z(x, y, 0), \quad p(x, y, 0) = 0.1, \end{aligned}$$

where $\zeta = x \cos \alpha + y \sin \alpha$, $\kappa = \sqrt{1 + \rho h \gamma^2}$, and corresponding exact solutions are

$$\begin{aligned} \rho(x, y, t) &= 1, \quad v_x(x, y, t) = -0.1 \sin(2\pi(\zeta + t/\kappa)) \sin \alpha, \\ v_y(x, y, t) &= 0.1 \sin(2\pi(\zeta + t/\kappa)) \cos \alpha, \quad v_z(x, y, t) = 0.1 \cos(2\pi(\zeta + t/\kappa)), \end{aligned}$$

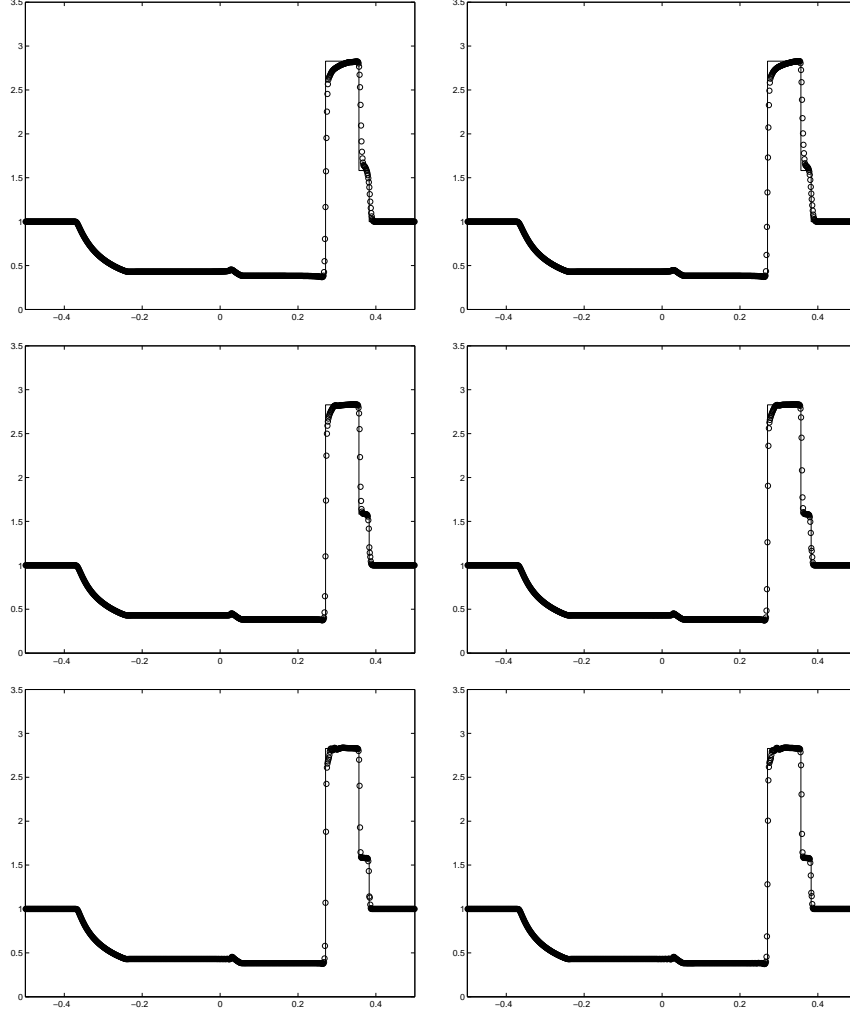


Figure 5.5. Example 5.3: The densities ρ at $t = 0.4$. The solid line denotes the exact solution, while the symbol “o” is numerical solution obtained with 800 cells. Left: P^K -based non-central DG methods; right: P^K -based central DG methods. From top to bottom: $K = 1, 2, 3$.

$$\begin{aligned} B_x(x, y, t) &= \cos \alpha + \kappa v_x(x, y, t), & B_y(x, y, t) &= \sin \alpha + \kappa v_y(x, y, t), \\ B_z(x, y, t) &= \kappa v_z(x, y, t), & p(x, y, t) &= 0.1. \end{aligned}$$

In the present computations, the fourth-order Runge-Kutta method mentioned in [58] is used in order to ensure the accuracy in time. The CFL numbers of P^1 -, P^2 -, and P^3 -based non-central DG methods are 0.2, 0.15, 0.1, respectively, and the CFL numbers for corresponding central DG methods are 0.3, 0.25, 0.2, respectively, and $\theta = \Delta t_n / \tau_n = 1$. Table 5.2 lists l^1 errors and orders in B_x obtained by the non-central and central DG methods. As can be seen from the table, two kinds of DG methods have reached the expected convergence orders.

Example 5.6 (Orszag-Tang problem) This RMHD Orszag-Tang problem is an extension of the non-relativistic version. The computational domain is chosen as $\Omega =$

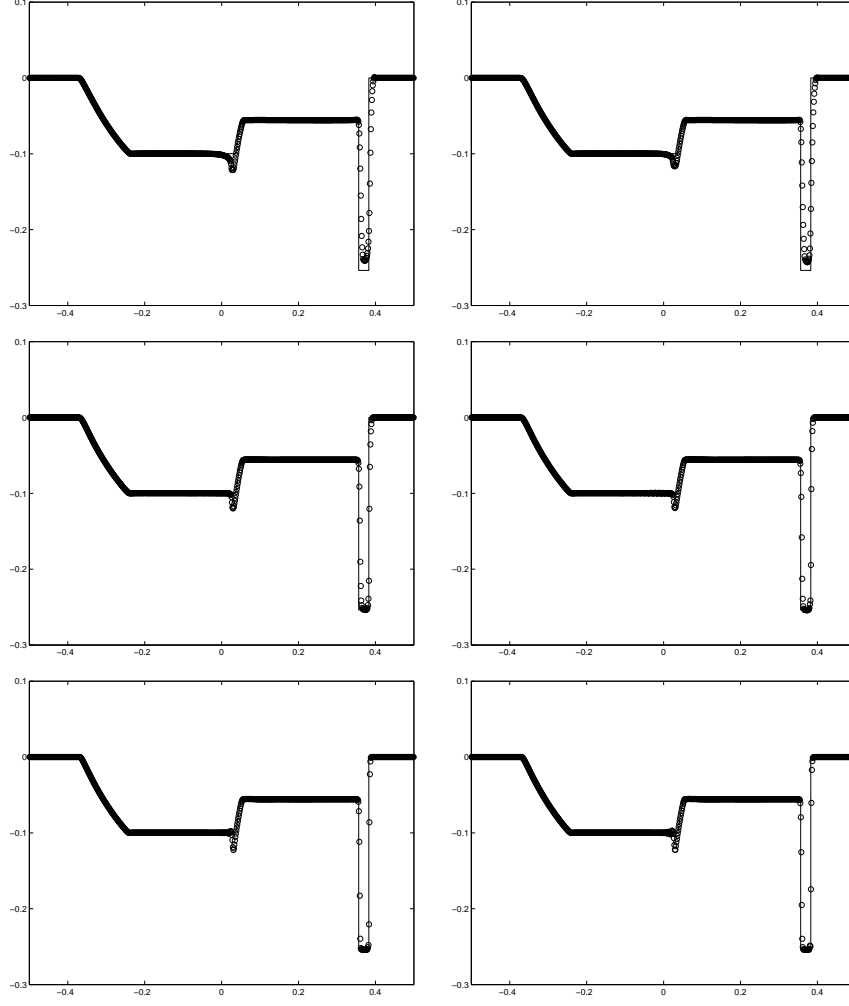


Figure 5.6. Same as Fig. 5.5 except for v_y .

$[0, 1] \times [0, 1]$, and the initial data are

$$\begin{aligned} \rho(x, y, 0) &= \frac{25}{36\pi}, \quad v_x(x, y, 0) = 0.5 \sin(2\pi y), \quad v_y(x, y, 0) = 0.5 \sin(2\pi x), \\ v_z(x, y, 0) &= 0, \quad B_x(x, y, 0) = -\frac{1}{\sqrt{4\pi}} \sin(2\pi y), \quad B_y(x, y, 0) = \frac{1}{\sqrt{4\pi}} \sin(4\pi x), \\ B_z(x, y, 0) &= 0, \quad p(x, y, 0) = \frac{5}{12\pi}, \end{aligned}$$

with the adiabatic index $\Gamma = 5/3$. The solution of problem is smooth initially, but the complicated wave structure is formed as the time increases, and it has the turbulence behavior.

The CFL numbers of P^1 -, P^2 -, and P^3 -based non-central DG methods are 0.2, 0.15, 0.1, respectively, while those of corresponding central DG methods are chosen as 0.3, 0.25, 0.2, respectively, and $\theta = \Delta t_n / \tau_n = 1$.

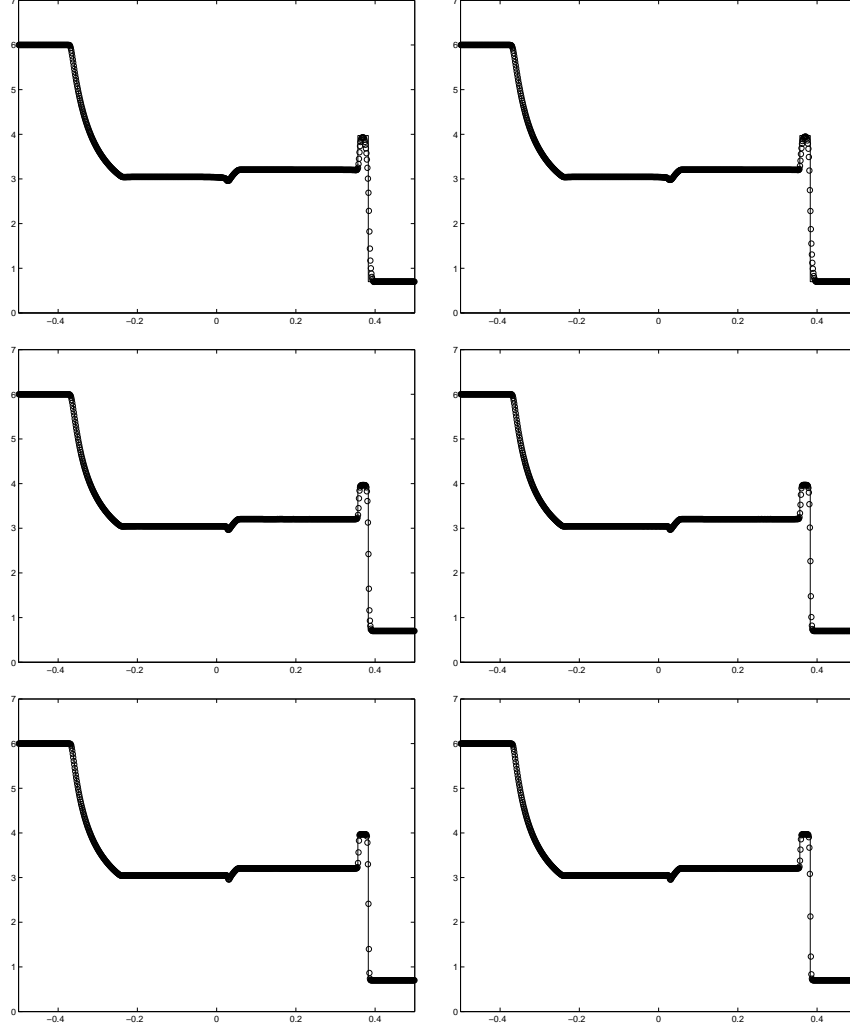


Figure 5.7. Same as Fig. 5.5 except for B_y .

Figs. 5.13 and 5.14 show the contours of densities ρ and Lorentz factors γ at $t = 1$ obtained by using the proposed DG methods with 200×200 cells. Fig. 5.15 plots them and the reference solutions along the line $y = 1 - x$, where the reference solutions are obtained by using the MUSCL scheme with 600×600 uniform cells. It is seen that the solutions obtained by higher-order DG methods are in good agreement with the reference solutions. The distribution of identified “troubled” cells is also consistent with the solutions, see Fig. 5.16.

Example 5.7 (Blast problem) It has become a very useful test for the multidimensional numerical schemes. Our setup is the same as that in [36]. The adiabatic index Γ and computational domain are taken as $4/3$ and $\Omega = [-0.5, 0.5] \times [-0.5, 0.5]$ with four outflow conditions, respectively. Initially, the magnetic field is constant, the fluid velocity is zero everywhere, and there is an explosion region with radius one at the

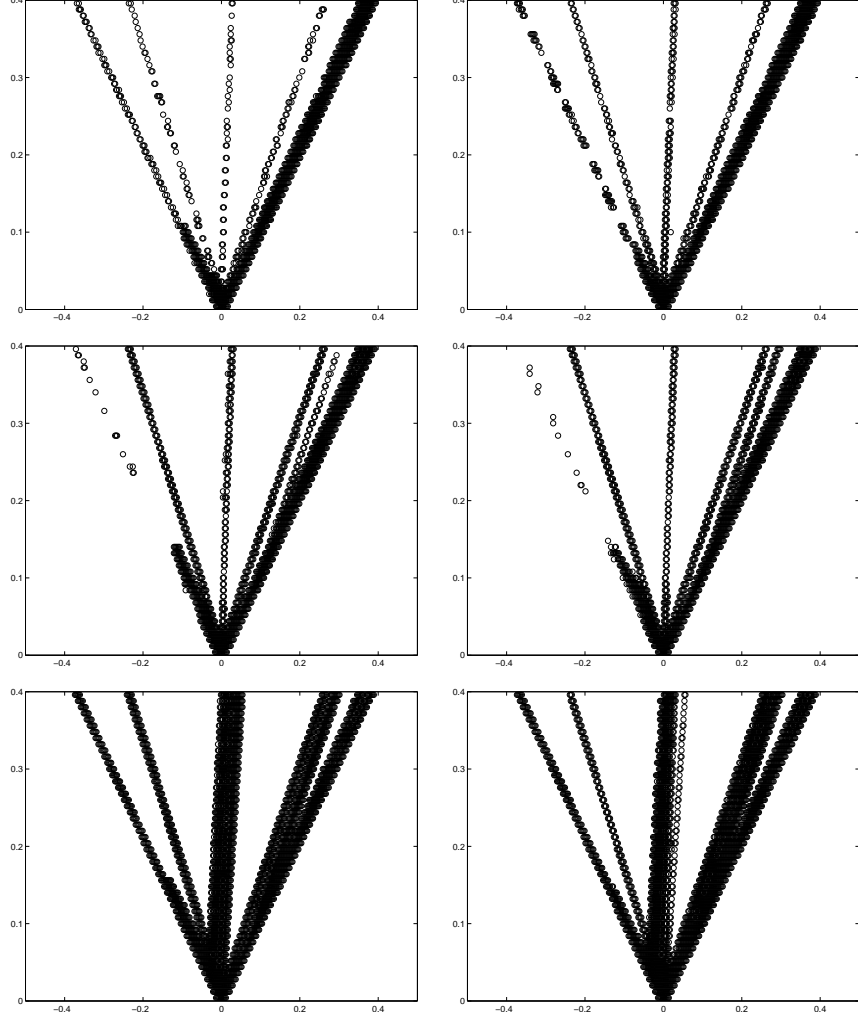


Figure 5.8. Example 5.3: The time evolution of “troubled” cells. Left: non-central DG methods; right: central DG methods. From top to bottom: $K = 1, 2, 3$. The cell number is 800.

center of Ω . The detailed description of initial data is as follows

$$(\rho, v_x, v_y, v_z, B_x, B_y, B_z, p) = \begin{cases} (1, 0, 0, 0, 0.05, 0, 0, 1), & r < 0.2, \\ (1, 0, 0, 0, 0.05, 0, 0, 10^{-3}), & r \geq 0.2, \end{cases}$$

where $r = \sqrt{x^2 + y^2}$.

Figs. 5.17 and 5.18 give the densities ρ and magnetic fields B_x at $t = 0.3$ obtained by the proposed DG methods with 300×300 cells, while Figs. 5.19 and 5.20 show them along the line $x = 0$ and the reference solutions, which are obtained by using the MUSCL scheme with 800×800 uniform cells. The CFL numbers of P^1 -, P^2 -, and P^3 -based non-central DG methods have been chosen as 0.2, 0.15, 0.1, respectively, while those of corresponding central DG methods are 0.3, 0.25, 0.2, and $\theta = \Delta t_n / \tau_n = 1$. As can be seen from those plots, the higher order methods can better resolve the discontinuities,

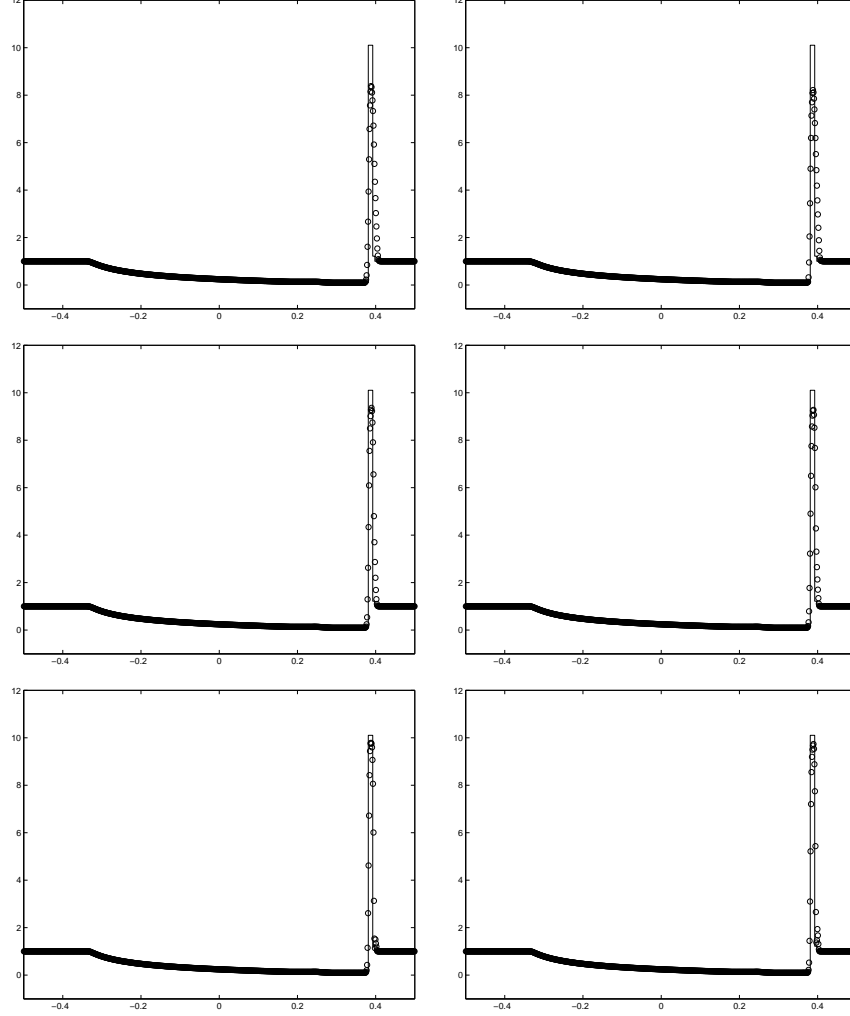


Figure 5.9. Example 5.4: The densities ρ at $t = 0.4$. The solid line denote the exact solution, while the symbol “o” is numerical solution obtained with 800 cells. Left: P^K -based non-central DG methods; right: P^K -based central DG methods. From top to bottom: $K = 1, 2, 3$.

and the numerical solutions are in good agreement with the reference solutions. Table 5.3 records the percentage of “troubled” cells, and shows that the “troubled” cells of relatively limited are identified.

Example 5.8 (Rotor problem) This problem is a relativistic extension of the classical MHD rotor test problem [64] and has been considered in the literature. The computational domain is $[-0.5, 0.5] \times [-0.5, 0.5]$ with four outflow conditions. Initially, the gas pressure and the magnetic field are uniform, and there is a disk of fluid centered at $(0, 0)$ and with high density rotating in a anti-clockwise direction at a high relativistic speed. The disk radius is 0.1. The ambient fluid is homogeneous for $r > 0.115$ and changing linearly for $0.1 \leq r \leq 0.115$, where $r = \sqrt{x^2 + y^2}$. Specifically, the initial data

Table 5.2

Example 5.5 l^1 errors in B_x and orders at $t = 1$ obtained by non-central and central DG methods. The fourth-order accurate Runge-Kutta method and $N \times 2N$ uniform cells are used.

		without limiter				with limiter in global			
		non-central DG		central DG		non-central DG		central DG	
	N	l^1 error	order	l^1 error	order	l^1 error	order	l^1 error	order
P^1	10	4.03e-03	—	3.48e-03	—	4.05e-02	—	3.65e-02	—
	20	6.99e-04	2.53	4.51e-04	2.95	1.27e-02	1.68	1.18e-02	1.63
	40	1.46e-04	2.25	5.98e-05	2.91	4.70e-03	1.43	4.35e-03	1.44
	80	3.37e-05	2.12	9.54e-06	2.65	1.29e-03	1.86	1.20e-03	1.86
	160	8.19e-06	2.04	1.72e-06	2.47	3.27e-04	1.98	3.03e-04	1.98
	320	2.03e-06	2.02	4.11e-07	2.07	8.07e-05	2.02	7.28e-05	2.06
P^2	10	3.11e-04	—	8.01e-04	—	2.93e-03	—	8.39e-03	—
	20	3.87e-05	3.01	9.81e-05	3.03	1.22e-04	4.59	6.69e-04	3.65
	40	4.83e-06	3.00	1.22e-05	3.01	1.03e-05	3.57	5.37e-05	3.64
	80	6.08e-07	2.99	1.52e-06	3.00	1.83e-06	2.49	5.74e-06	3.23
	160	7.74e-08	2.97	1.89e-07	3.00	2.48e-07	2.89	6.90e-07	3.06
	320	9.87e-09	2.97	2.37e-08	3.00	3.16e-08	2.97	8.56e-08	3.01
P^3	10	2.18e-05	—	3.32e-05	—	5.51e-04	—	5.68e-04	—
	20	1.77e-06	3.62	2.23e-06	3.90	1.06e-05	5.70	1.57e-05	5.17
	40	1.03e-07	4.10	1.43e-07	3.97	2.44e-07	5.43	6.96e-07	4.50
	80	5.67e-09	4.19	8.97e-09	3.99	1.10e-08	4.47	4.25e-08	4.04
	160	3.11e-10	4.19	5.62e-10	4.00	6.44e-10	4.10	2.69e-09	3.98
	320	1.89e-11	4.04	3.51e-11	4.00	4.00e-11	4.01	1.70e-10	3.98

Table 5.3

The percentage of “troubled” cells identified by non-central and central DG methods.

	Example 5.7		Example 5.8		Example 5.9	
	non-central	central	non-central	central	non-central	central
P^1	3.52	5.42	0.61	8.18	8.81	8.58
P^2	9.15	10.2	12.5	14.5	20.5	17.1
P^3	11.8	13.0	16.7	18.8	26.3	27.4

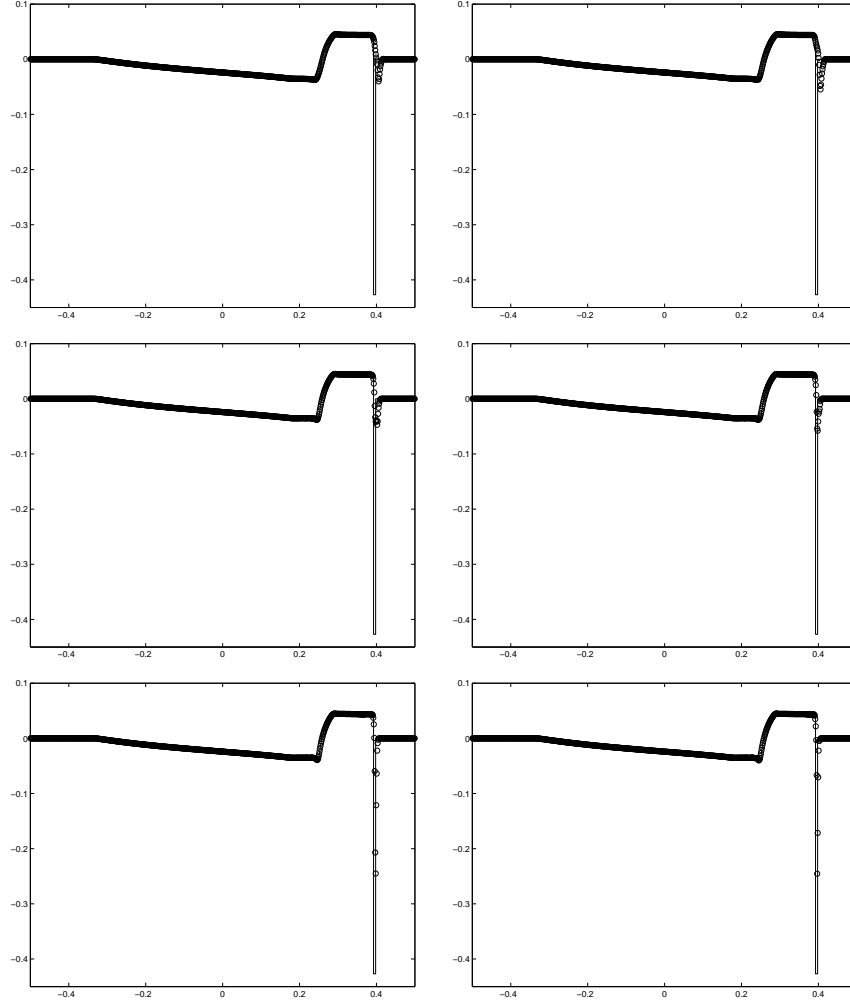


Figure 5.10. Same as Fig. 5.9 except for the the velocity v_y .

Table 5.4

CPU times of non-central and central DG methods (second).

	Example 5.7		Example 5.8		Example 5.9	
	non-central	central	non-central	central	non-central	central
P^1	1.12e5	2.11e5	2.81e5	6.25e5	1.76e6	3.44e6
P^2	5.52e5	8.00e5	6.55e5	1.84e6	3.56e6	1.10e7
P^3	1.16e6	2.59e6	1.73e6	5.98e6	1.10e7	2.25e7

are taken as

$$(\rho, v_x, v_y, v_z, B_x, B_y, B_z, p) = \begin{cases} (10, -\alpha y, \alpha x, 0, 1, 0, 0, 1), & r < 0.1, \\ (1 + 9\delta, -\alpha y\delta/r, \alpha x\delta/r, 0, 1, 0, 0, 1), & 0.1 \leq r \leq 0.115, \\ (1, 0, 0, 0, 1, 0, 0, 1), & r > 0.115, \end{cases}$$

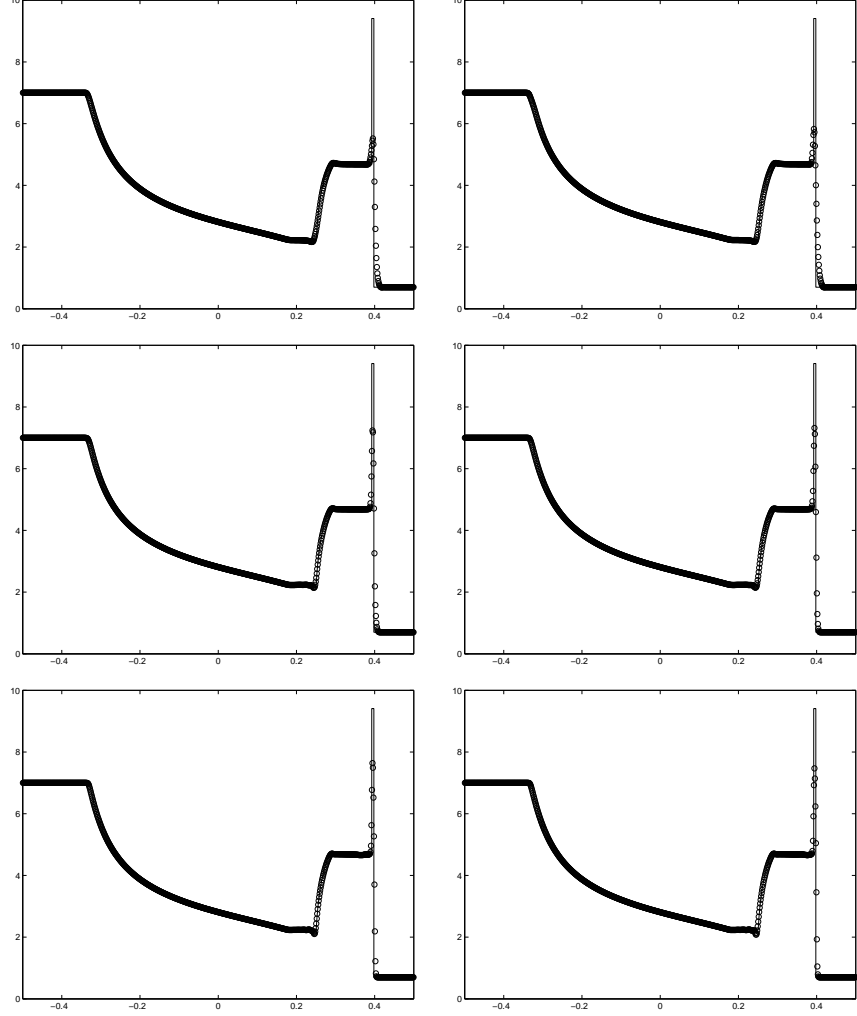


Figure 5.11. Same as Fig. 5.9 except for the magnetic field B_y .

where $\alpha = 9.95$, $\delta(r) := (0.115 - r)/0.015$ is a “taper” function helping to reduce initial transients. The adiabatic index is taken as $\Gamma = 5/3$.

Figs. 5.21, 5.22, 5.23, and 5.24 show respectively the contour plots of density ρ , gas pressure p , magnetic pressure p_m , and Lorentz factor γ at $t = 0.4$ obtained by using DG methods with 300×300 cells. The CFL numbers of P^1 -, P^2 -, P^3 -based non-central DG methods are 0.2, 0.15, 0.1, respectively, while those of corresponding central DG are $0.3/\theta$, $0.25/\theta$, $0.2/\theta$ with $\theta = 0.3$, that is, $\Delta t_n = 0.3\tau_n$. The parameter M in the modified TVB minmod function is taken as $M = 500$. From those results, one can see that as the time increases, the winding magnetic field lines are formed and decelerated the disk speed, and the initial high density at the center is swept away completely and a oblong-shaped shell is formed. At $t = 0.4$, the central magnetic field lines are rotated almost 90° . Those computed results agree quite well with other published solutions. Fig. 5.25 gives a comparison of the density and gas pressure at $t = 0.4$ along the line $y = x$ to the reference solutions, which are obtained by using the MUSCL scheme

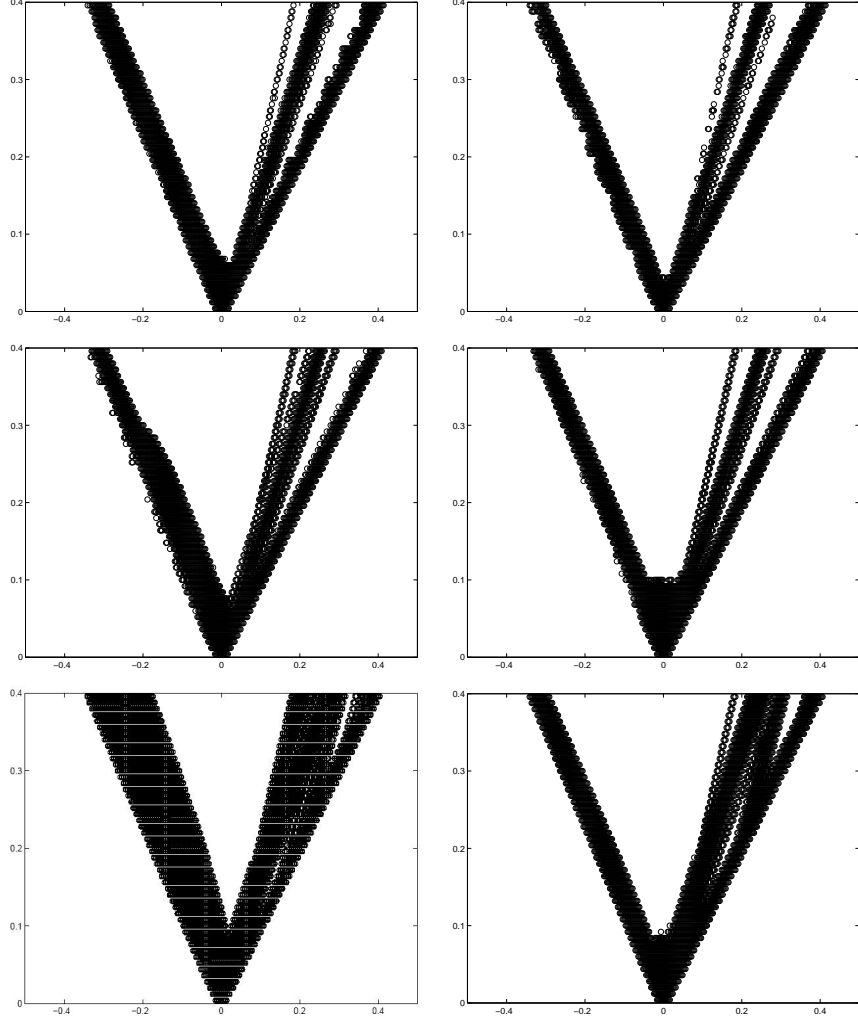


Figure 5.12. Example 5.4: The time evolution of “troubled” cells. Left: non-central DG methods; right: central DG methods. From top to bottom: $K = 1, 2, 3$. The cell number is 800.

with 800×800 uniform cells. It is seen that the resolution of central DG methods is slightly better than corresponding non-central DG methods, and the numerical solution of the high order methods is in good agreement with the reference solution. Moreover, high order methods identify more “troubled” cells, see Table 5.3 for the percentage of troubled cells. Corresponding CPU times given in Table 5.4 show that the CPU time used in central DG methods is significantly more than that of the same order non-central DG methods.

Example 5.9 (Shock and cloud interaction) The shock-cloud interaction problem modeling the disruption of a high density cloud by a strong shock wave has been widely used to test the classical MHD codes, see e.g. [19,47,51]. It is extended to the relativistic case with the magnetic field orthogonal to the slab plane in [39] so that any magnetic divergence-free treatment is not needed. Here we consider a different extension of this problem [23], in which the magnetic field is not orthogonal to the slab plane so that

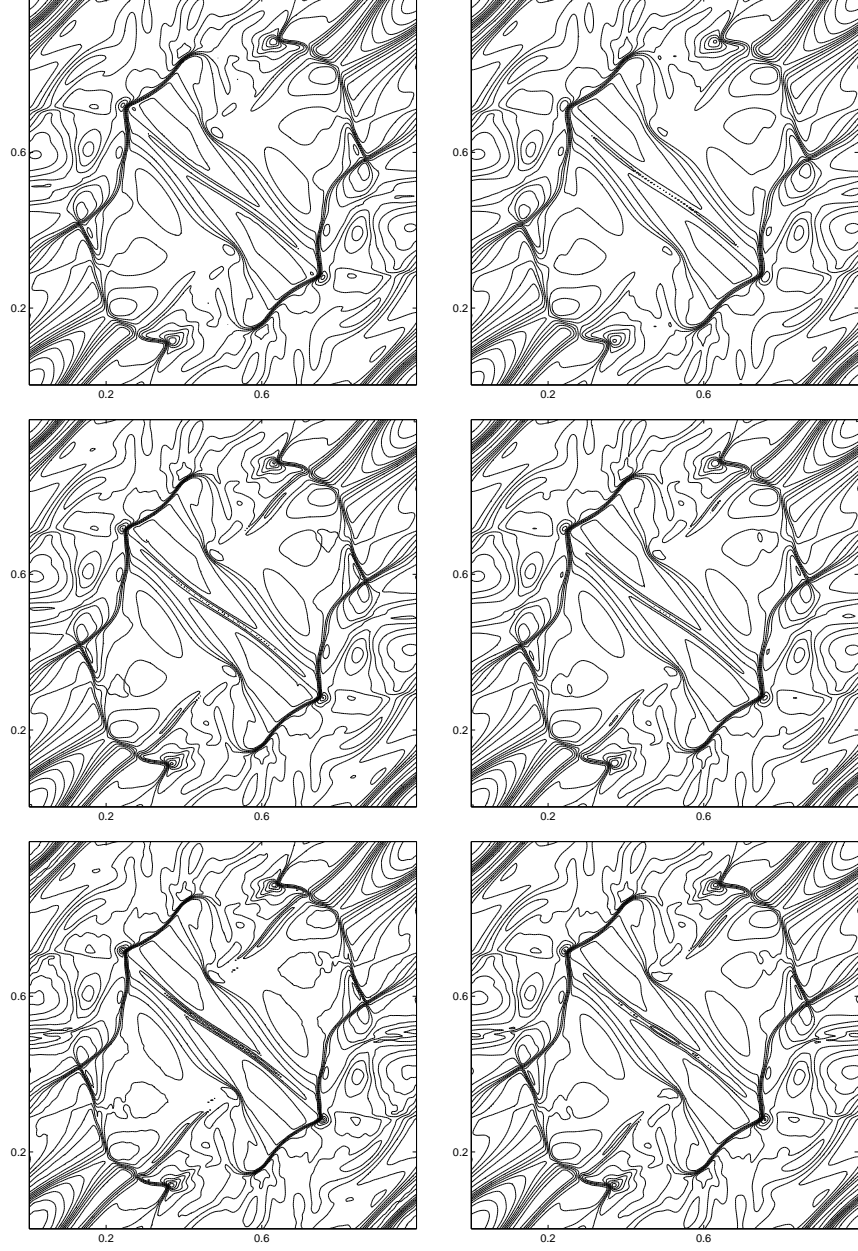


Figure 5.13. Example 5.6 The contour plots of density ρ at $t = 1$ obtained by using 200×200 cells (15 equally spaced contour lines from 0.06 to 0.48). Left: P^K -based DG methods; right: P^K -based central DG methods. From top to bottom: $K = 1, 2, 3$.

the magnetic divergence-free treatment has to be imposed. The adiabatic index Γ and computational domain are $5/3$ and $[-0.2, 1.2] \times [0, 1]$, respectively. The inflow condition is specified on the left boundary, while the outflow conditions are on other boundaries. Initially, there is a right-moving shock wave located at $x = 0.05$ and with the left and right states

$$(\rho, v_x, v_y, v_z, B_x, B_y, B_z, p)(x, y, 0)$$

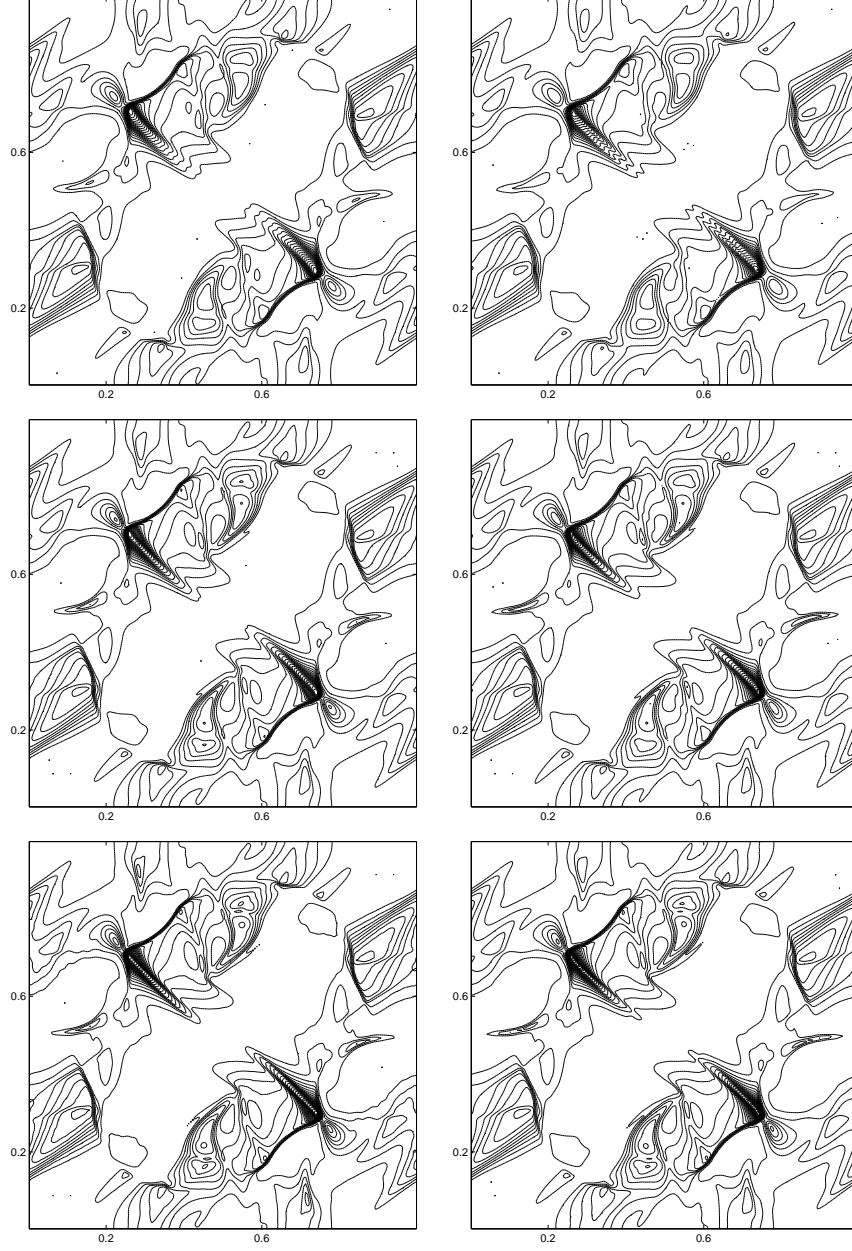


Figure 5.14. Same as Fig. 5.13 except for the Lorentz factor γ (30 equally spaced contour lines from 1 to 2.2).

$$= \begin{cases} (3.86859, 0.68, 0, 0, 0, 0.84981, -0.84981, 1.25115), & x < 0.05, \\ (1, 0, 0, 0, 0, 0.16106, 0.16106, 0.05), & x > 0.05. \end{cases}$$

There exists a rest circular cloud which is in magneto-hydrostatic balance with the surrounding fluid and centered at the point $(0.25, 0.5)$ with a high density $\rho = 30$ and radius 0.15.

Figs. 5.26 and 5.27 show the the densities ρ and magnetic pressures p_m at $t = 1.2$

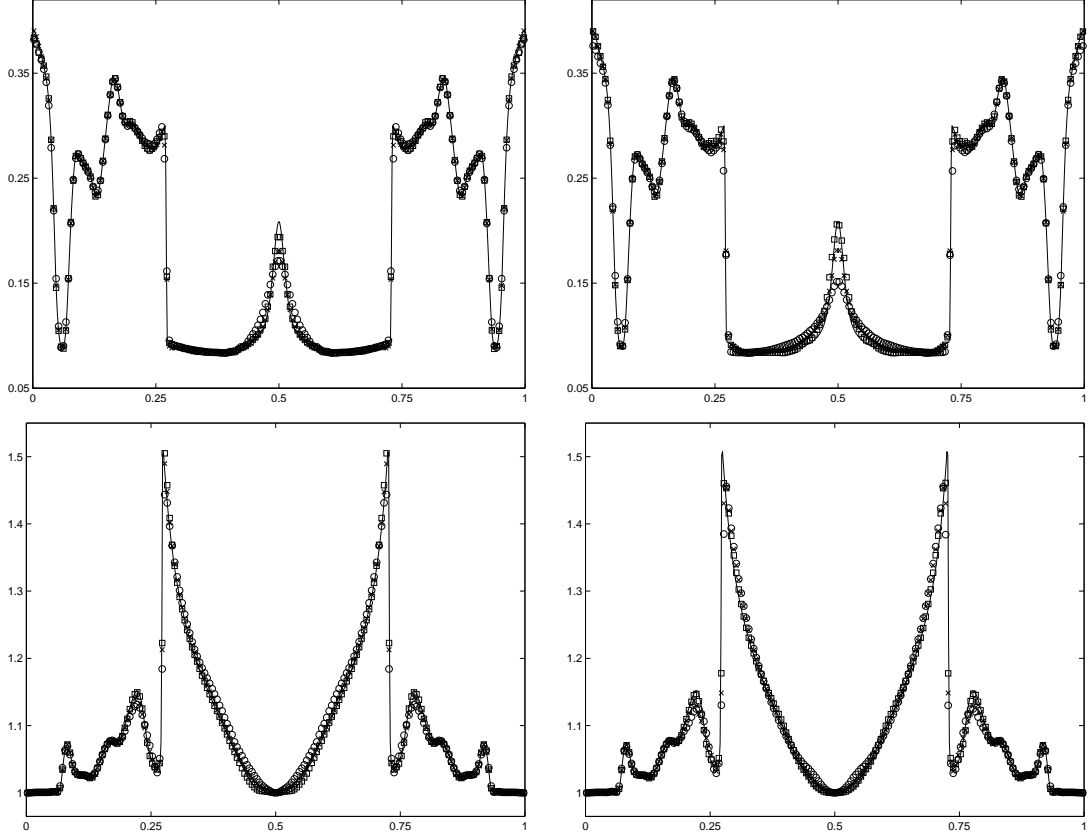


Figure 5.15. Example 5.6: The densities ρ (top) and Lorentz factors γ (bottom) at $t = 1$ along the line $y = 1 - x$. The solid line denotes the reference solution obtained by using the MUSCL scheme with 600×600 cells, while the symbols “o”, “x”, and “□” denote the numerical solutions obtained by using the P^1 -, P^2 -, and P^3 methods with 200×200 cells. Left: DG methods; right: central DG methods.

obtained by the proposed DG methods with 420×300 cells. The CFL numbers of P^1 -, P^2 -, P^3 -based non-central DG methods are 0.2, 0.15, 0.1, respectively, while those of corresponding central DG methods are $0.3/\theta$, $0.25/\theta$, $0.2/\theta$, with $\theta = 0.3$, that is, $\Delta t_n = 0.3\tau_n$. One can see from those plots that compared to the low order methods, high order methods better capture the reflected wave structure and resolved the complex wave structure generated due to the interaction between the shock wave and cloud, while the number of “troubled” cells identified by the higher order methods is larger, see Table 5.3. Fig. 5.29 displays the densities ρ and magnetic pressures p_m at $t = 1.2$ along $y = 0.5$. It finds the good agreement between the numerical solutions obtained by the higher order methods and the reference solutions, which are obtained by using the MUSCL scheme with 980×700 uniform cells. The solutions of higher order methods are obviously better than the low order methods.

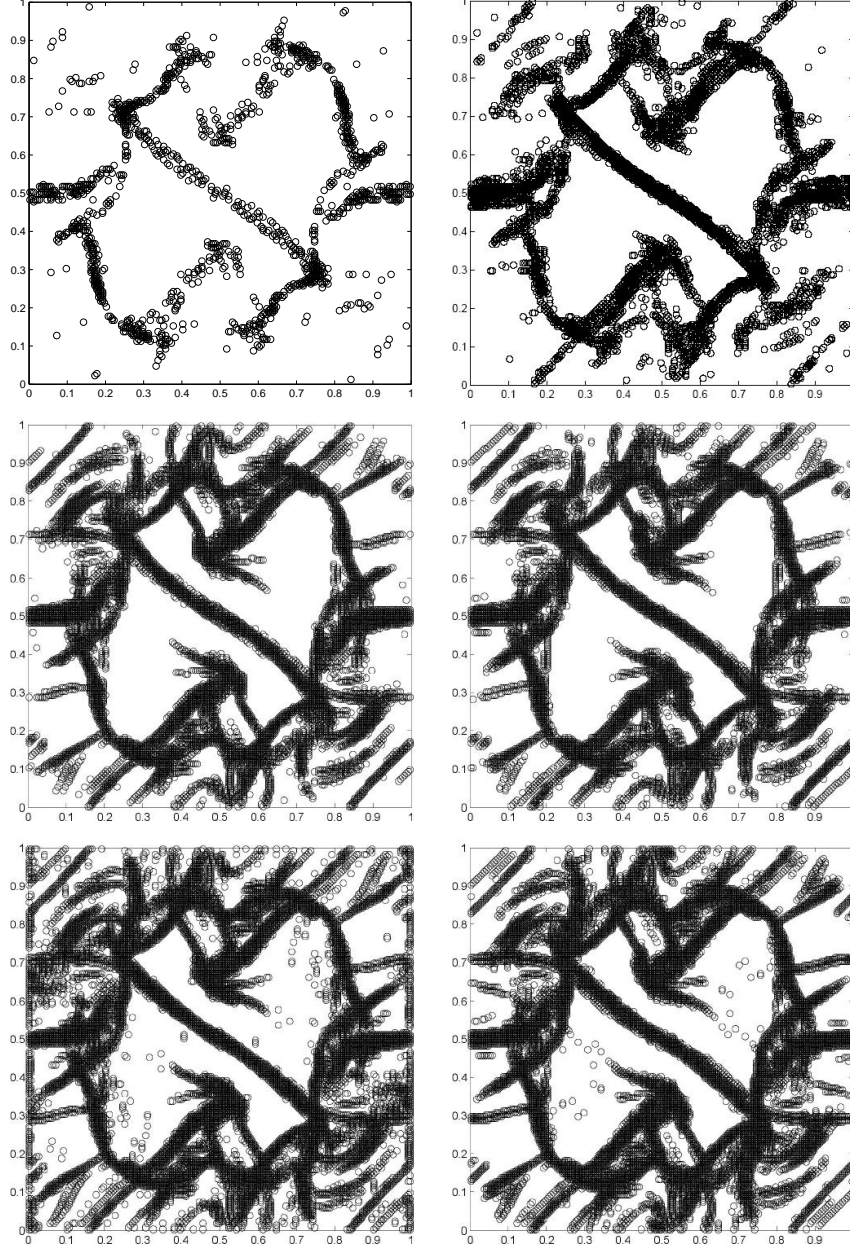


Figure 5.16. Same as Fig. 5.13 except for the “troubled” cells.

6 Conclusions

The paper developed Runge-Kutta P^K -based non-central and central DG methods with WENO limiter to the one- and two-dimensional special relativistic magnetohydrodynamical (RMHD) equations, $K = 1, 2, 3$. The non-central DG methods were locally divergence-free, while the central DG methods were “exactly” divergence-free but had to find two approximate solutions defined on mutually dual meshes. For each mesh, the central DG approximate solutions on its dual mesh were used to calculate the flux

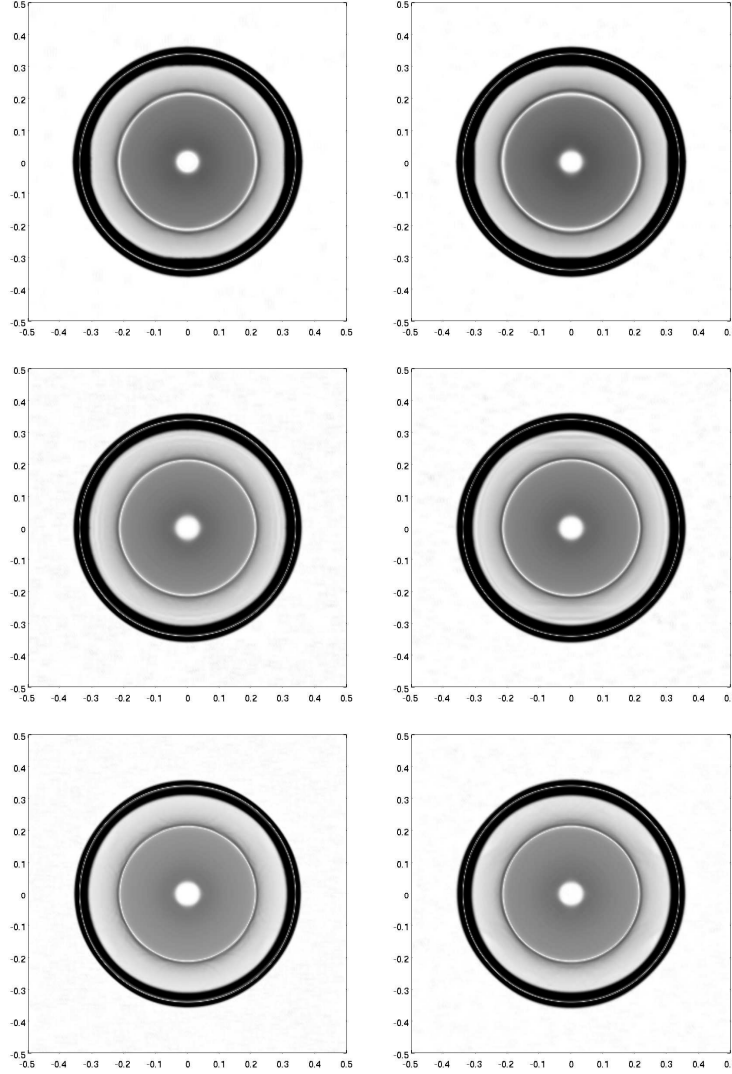


Figure 5.17. Example 5.7: Schlieren images of density ρ at $t = 0.3$ obtained with 300×300 cells. Left: P^K -based RKDG methods; right: P^K -based Runge-Kutta CDG methods. From top to bottom: $K = 1, 2, 3$.

values in the cell and on the cell boundary so that the approximate solutions on mutually dual meshes were coupled with each other, and the use of numerical flux might be avoided. In addition the central DG methods allowed the use of a larger CFL number. The adaptive WENO limiter was directly implemented for the physical variables $\mathbf{R} = (D, m_x, m_y, m_z, B_z, E)^T$ by two steps: the “troubled” cells were first identified by using a modified TVB minmod function, and then new polynomials of degree $(2K + 1)$ inside the “troubled” cells were locally reconstructed to replace the non-central or central DG solutions by using the WENO technique based on the cell average values of the DG solutions in the neighboring cells as well as the original cell averages of the “troubled” cells.

However, in order that the WENO limiting procedure did not destroy the locally or “ex-

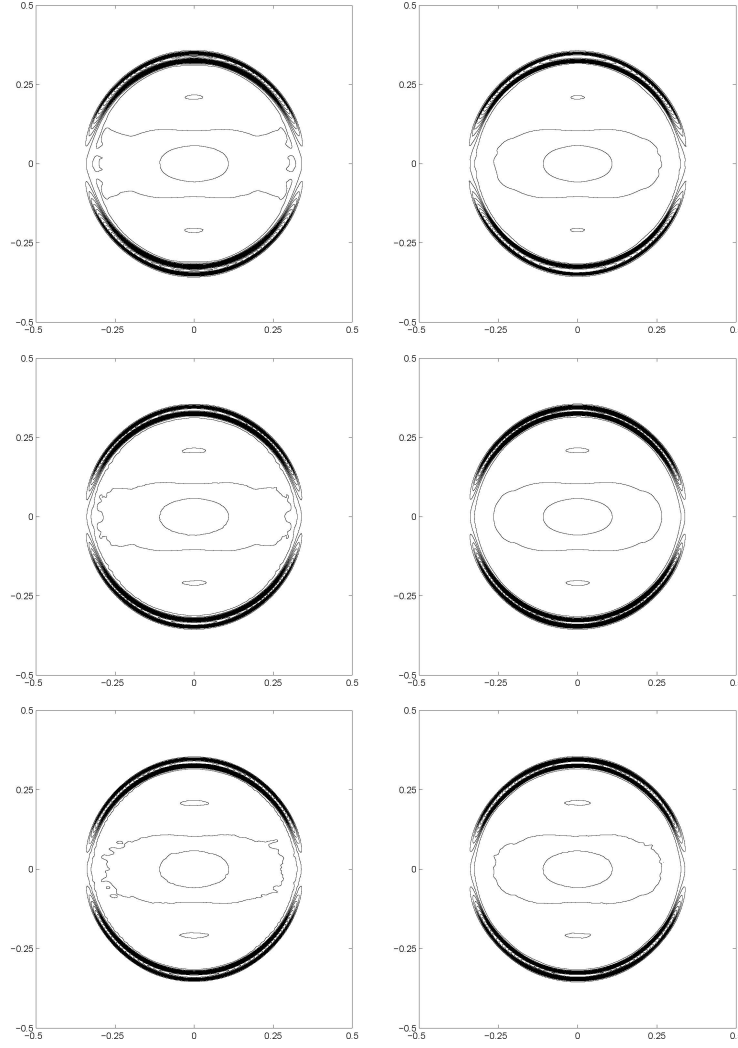


Figure 5.18. Same as Fig. 5.17 except for the magnetic field B_x (15 equally spaced contour lines from 0.02 to 0.35).

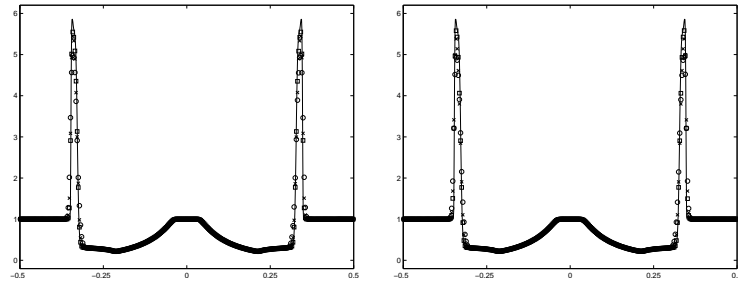


Figure 5.19. Example 5.7: The density ρ at $t = 0.3$ along the line $x = 0$. The solid line denote the reference solution obtained by using the MUSCL scheme with 800×800 cells, while the symbol “o”, “ \times ”, and “ \square ” denote the solutions obtained by using the P^1 -, P^2 -, and P^3 -based methods with 300×300 cells respectively. Left: DG methods; right: central DG methods.

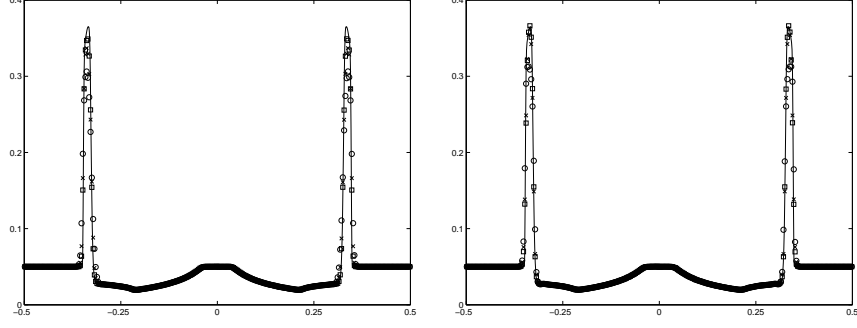


Figure 5.20. Same as Fig. 5.19 except for the magnetic field B_x along the line $x = 0$.

actly” divergence-free property of magnetic field, it should be specially implemented for the magnetic field $\mathbf{Q} = (B_x, B_y)^T$. In view of the fact that the non-central DG methods used a piecewise polynomial approximation of the magnetic field which satisfied the divergence free property locally, our WENO limiting procedure also used the polynomial satisfying the divergence free property to give a new approximation of the magnetic field so that the approximate magnetic field of non-central DG methods with WENO limiter is still locally divergence free. In the “exactly” divergence-free central DG methods, the approximated normal magnetic field was first obtained by solving the governing equation of magnetic field on the cell boundary, and then used to reconstruct the new magnetic field within the cell, which is locally divergence-free in the cell and whose normal component was continuous across the cell boundary. Thus the WENO limiting procedure was first applied to the approximated normal magnetic field on the cell boundary and then the “exactly” divergence-free WENO magnetic field is reconstructed. Because the WENO limiter was only employed for finite “troubled” cells, the computational cost can be as little as possible.

Several test problems in one and two dimensions were solved by using our locally and “exactly” divergence-free DG methods with WENO limiter. The numerical results demonstrated that our methods were stable, accurate, and robust in resolving complex wave structures. From the results of two-dimensional examples, it was seen that the resolution of “exactly” divergence-free central DG methods was slightly higher than the local divergence free non-central DG methods, but the CPU times of central DG methods were longer. In solving RMHD problems with large Lorentz factor, or strong discontinuities, or low rest-mass density or pressure etc., it is still possible for the P^K -based non-central and central DG methods to give nonphysical solutions. To cure such difficulty, the P^0 -based methods may be locally used to replace the P^K -based. The genuinely effective way is to employ the physical-constraints preserving methods, see e.g. [57].

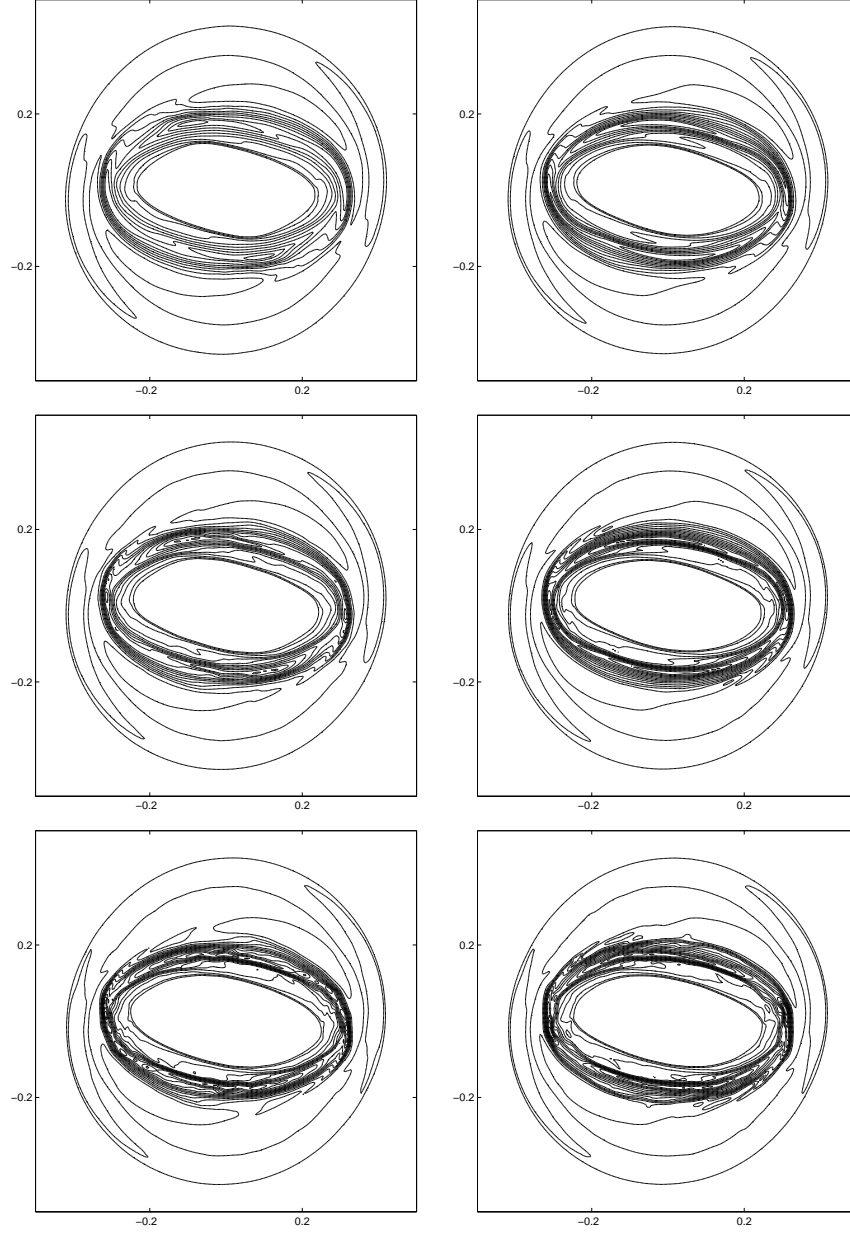


Figure 5.21. Example 5.8: The contour plots of density ρ at $t = 0.4$ obtained with 300×300 cells (15 equally spaced contour lines from 0.3 to 8.2). Left: P^K -based DG methods; right: P^K -based central DG methods. From top to bottom: $K = 1, 2, 3$.

Acknowledgements

This work was partially supported by the National Natural Science Foundation of China (Nos. 91330205 & 11421101).

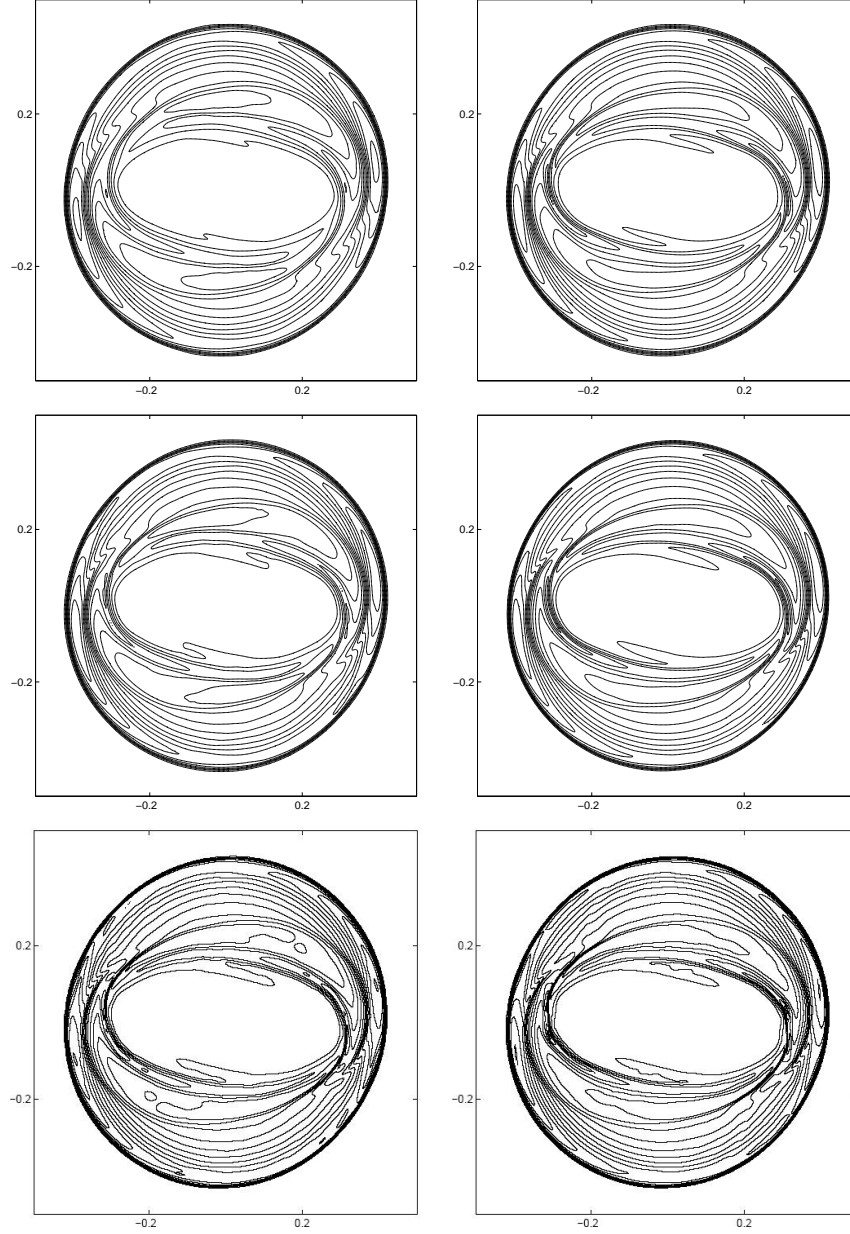


Figure 5.22. Same as Fig. 5.21 except for the gas pressure p (15 equally spaced contour lines from 0 to 4.2).

References

- [1] M. Anderson, E.W. Hirschmann, S.L. Liebling, and D. Neilsen. Relativistic MHD with adaptive mesh refinement. *Class. Quantum Grav.*, 23:6503-6524, 2006.
- [2] A.M. Anile. *Relativistic Fluids and Magneto-fluids: With Applications in Astrophysics and Plasma Physics*. Cambridge University Press, Cambridge, 1989.
- [3] A.M. Anile and S. Pennisi. On the mathematical structure of test relativistic

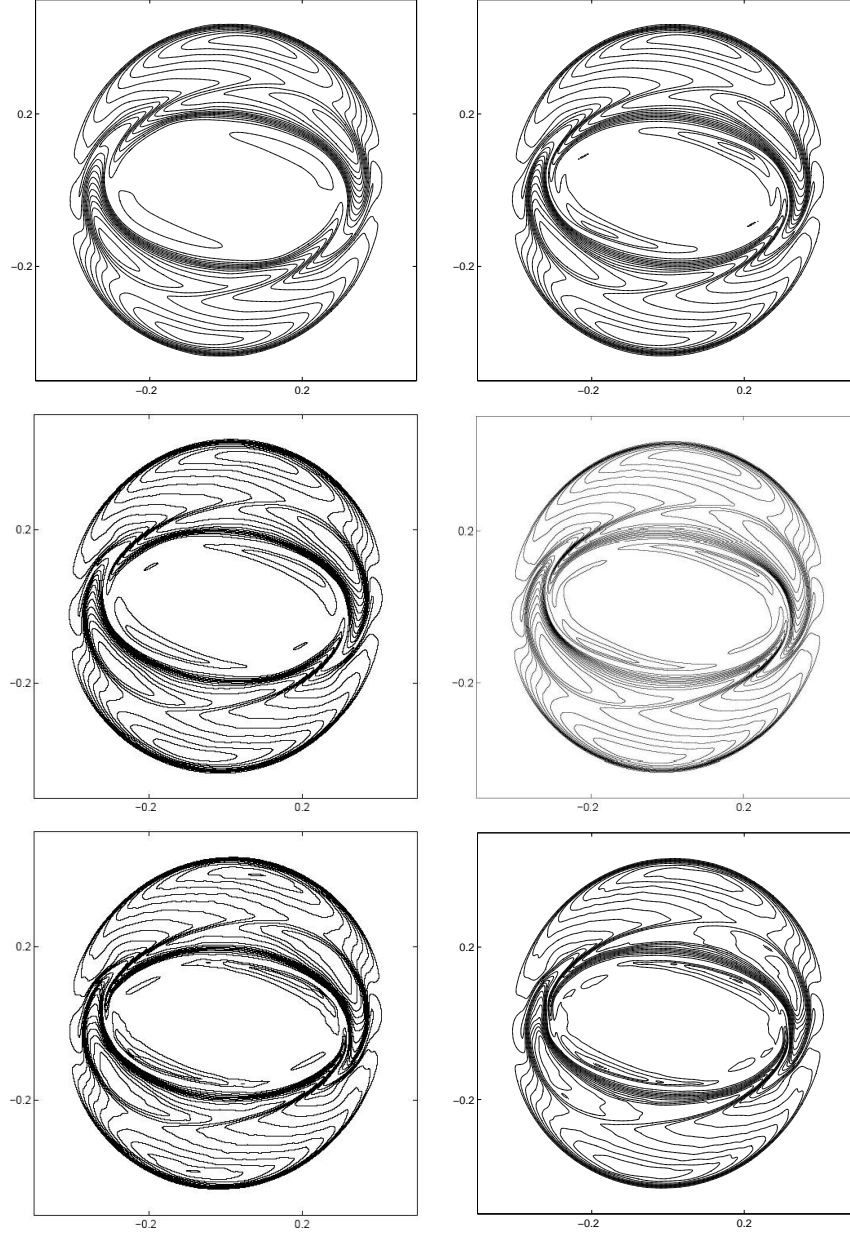


Figure 5.23. Same as Fig. 5.21 except for the magnetic pressure p_m (15 equally spaced contour lines from 0 to 2.1).

- magnetofluidynamics. *Ann. Inst. Henri Poincaré*, 46:27-44, 1987.
- [4] L. Antón, J.A. Miralles, J.M. Martí, J.M. Ibáñez, M.A. Aloy, and P. Mimica. Relativistic magnetohydrodynamics: renormalized eigenvectors and full wave decomposition Riemann solver. *Astrophys. J. Suppl. S.*, 188:1-31, 2010.
 - [5] D.S. Balsara. Total variation diminishing scheme for relativistic magnetohydrodynamics. *Astrophys. J. Suppl. S.*, 132:83-101, 2001.
 - [6] F. Bassi and S. Rebay. A high-order accurate discontinuous finite element method for the numerical solution of the compressible NavierStokes equations. *J. Comput. Phys.*,

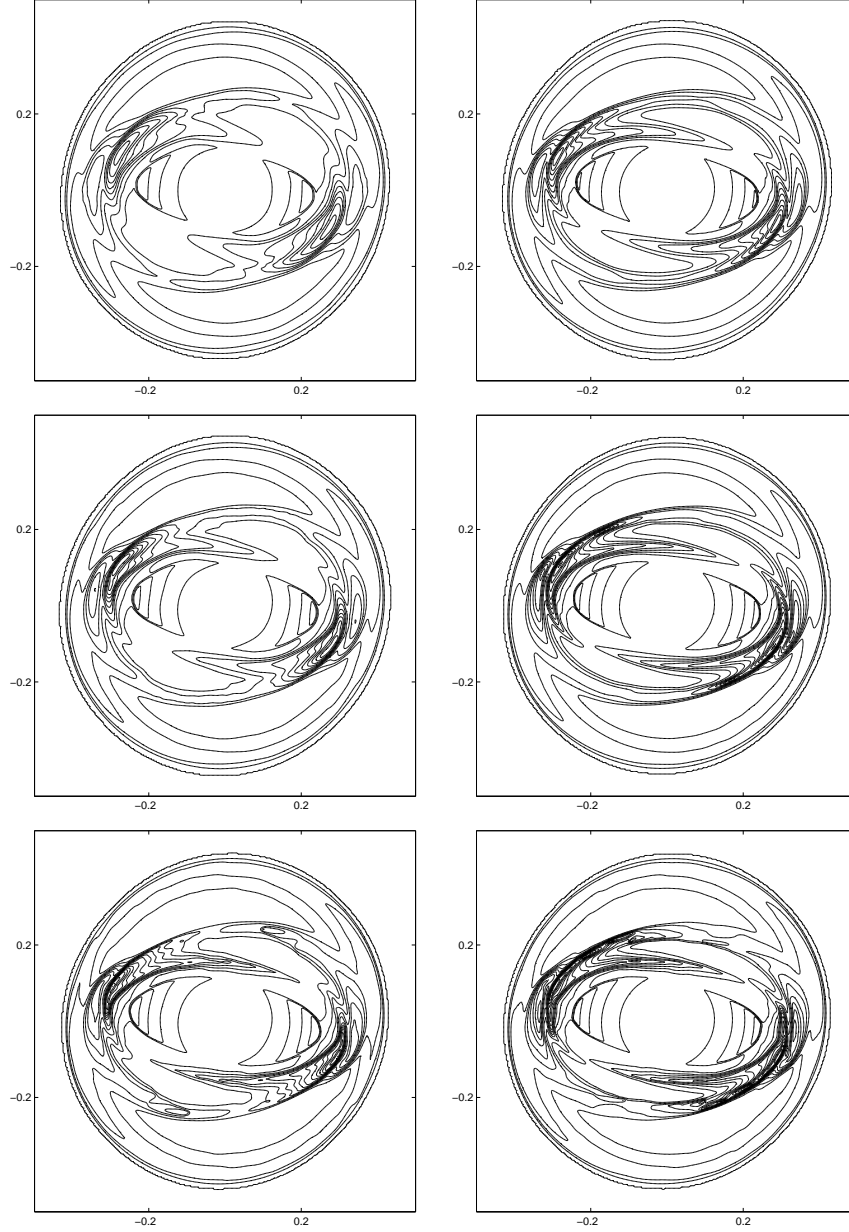


Figure 5.24. Same as Fig. 5.21 except for the Lorentz factor (15 equally spaced contour lines from 1 to 1.9).

131:267-279, 1997.

- [7] J. Bergmans, R. Keppens, D.E.A. van Odyck, and A. Achterberg. Simulations of relativistic astrophysical flows. In *Adaptive Mesh Refinement: Theory and Applications*, pages 223-233. Springer Berlin Heidelberg, 2005.
- [8] R. Biswas, K.D. Devine, and J.E. Flaherty. Parallel, adaptive finite element methods for conservation laws. *Appl. Numer. Math.*, 14:255-283, 1994.
- [9] J.U. Brackbill and D.C. Barnes. The effect of nonzero $\nabla \cdot \mathbf{B} = 0$ on the numerical solution of the magnetohydrodynamic equations. *J. Comput. Phys.*, 35:426-430, 1980.

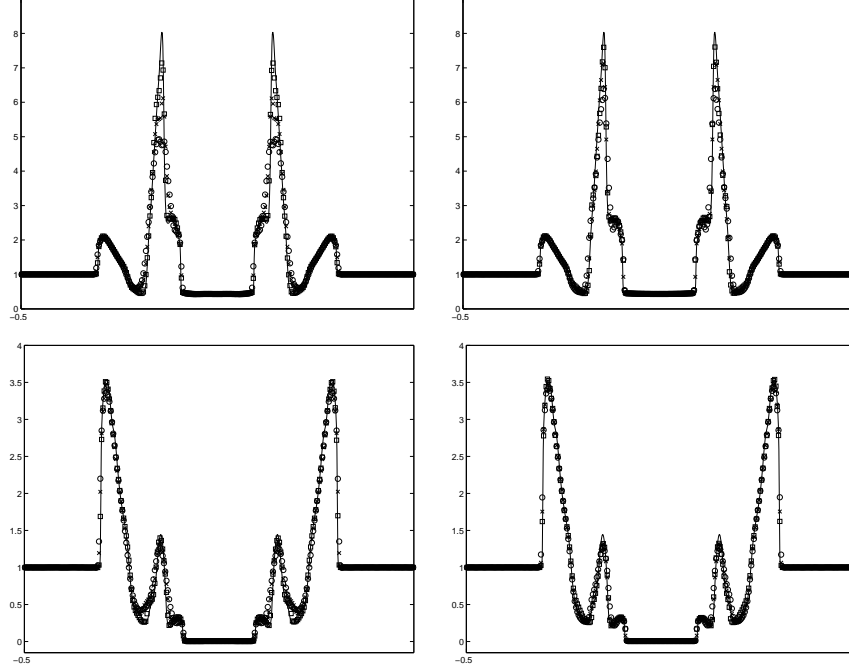


Figure 5.25. Example 5.8: The densities (top) and gas pressure p (bottom) at $t = 0.4$ along the line $y = x$. The solid line denotes the reference solution obtained by using the MUSCL scheme with 800×800 uniform cells, while the symbols “o”, “x”, and “□” denotes the numerical solutions obtained by the P^1 -, P^2 -, and P^3 -based methods with 300×300 cells, respectively.

- [10] M. Brio and C.C. Wu. An upwind differencing scheme for the equations of ideal magnetohydrodynamics. *J. Comput. Phys.*, 75:400-422, 1988.
- [11] B. Cockburn, S.C. Hu, and C.-W. Shu. The Runge-Kutta local projection discontinuous Galerkin finite element method for conservation laws IV: the multidimensional case. *Math. Comp.*, 54:545-581, 1990.
- [12] B. Cockburn, F.Y. Li, and C.-W. Shu. Locally divergence-free discontinuous Galerkin methods for the Maxwell equations. *J. Comput. Phys.*, 194:588-610, 2004.
- [13] B. Cockburn, S.Y. Lin, and C.-W. Shu. TVB Runge-Kutta local projection discontinuous Galerkin finite element method for conservation laws III: one-dimensional systems. *J. Comput. Phys.*, 84:90-113, 1989.
- [14] B. Cockburn and C.-W. Shu. TVB Runge-Kutta local projection discontinuous Galerkin finite element method for conservation laws II: general framework. *Math. Comp.*, 52:411-435, 1989.
- [15] B. Cockburn and C.-W. Shu. The Runge-Kutta local projection P^1 -discontinuous-Galerkin finite element method for scalar conservation laws. *RAIRO Modél. Math. Anal. Numér.*, 25:337-361, 1991.
- [16] B. Cockburn and C.-W. Shu. The local discontinuous Galerkin method for time-dependent convection-diffusion systems. *SIAM J. Numer. Anal.*, 35:2440-2463, 1998.
- [17] B. Cockburn and C.-W. Shu. The Runge-Kutta discontinuous Galerkin method for conservation laws V: multidimensional systems. *J. Comput. Phys.*, 141:199-224, 1998.

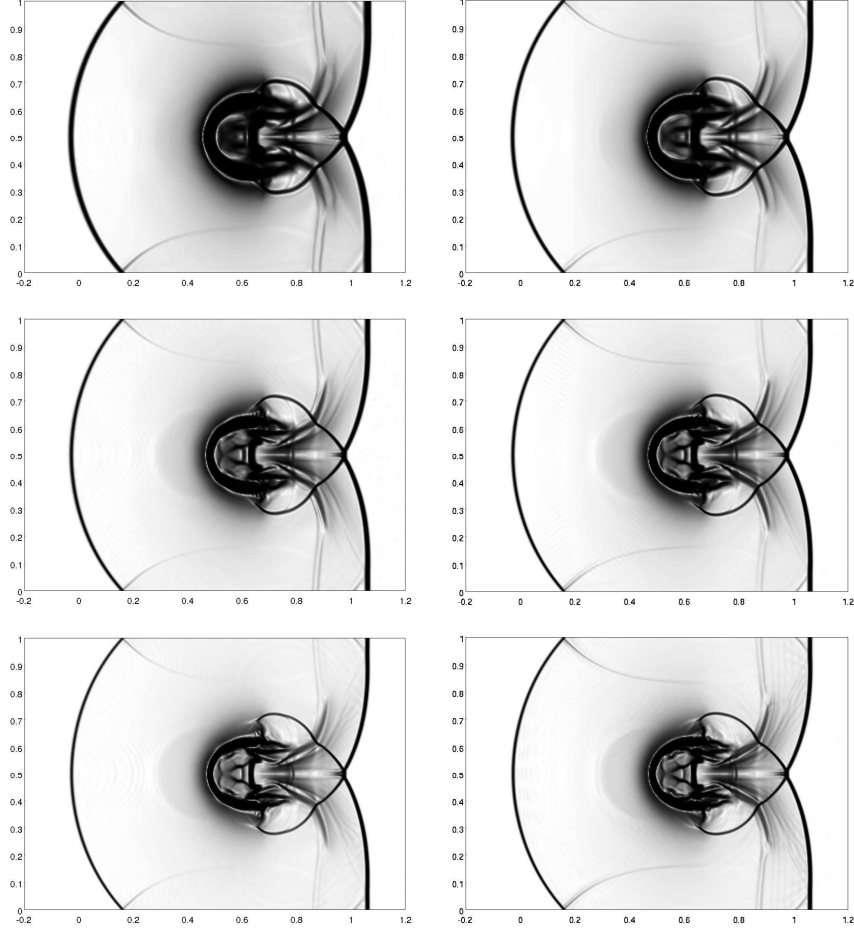


Figure 5.26. Example 5.9: Schlieren images of density ρ at $t = 1.2$ obtained with 420×300 cells. Left: P^K -based DG methods; right: P^K -based central DG methods. From top to bottom: $K = 1, 2, 3$.

- [18] B. Cockburn and C.-W. Shu. Runge-Kutta discontinuous Galerkin methods for convection-dominated problems. *J. Sci. Comput.*, 16:173-261, 2001.
- [19] W.L. Dai and P.R. Woodward. A simple finite difference scheme for multi-dimensional magnetohydrodynamical equations. *J. Comput. Phys.*, 142:331-369, 1998.
- [20] C.R. Evans and J.F. Hawley. Simulation of magnetohydrodynamic flows: A constrained transport method. *Astrophys. J.*, 332:659-677, 1988.
- [21] B. Giacomazzo and L. Rezzolla. The exact solution of the Riemann problem in relativistic magnetohydrodynamics. *J. Fluid Mech.*, 562:223-259, 2006.
- [22] P. He and H.Z. Tang. An adaptive moving mesh method for two-dimensional relativistic hydrodynamics. *Commun. Comput. Phys.*, 11:114-146, 2012.
- [23] P. He and H.Z. Tang. An adaptive moving mesh method for two-dimensional relativistic magnetohydrodynamics. *Computers & Fluids*, 60:1-20, 2012.
- [24] V. Honkkila and P. Janhunen. HLLC solver for ideal relativistic MHD. *J. Comput. Phys.*, 223:643-656, 2007.

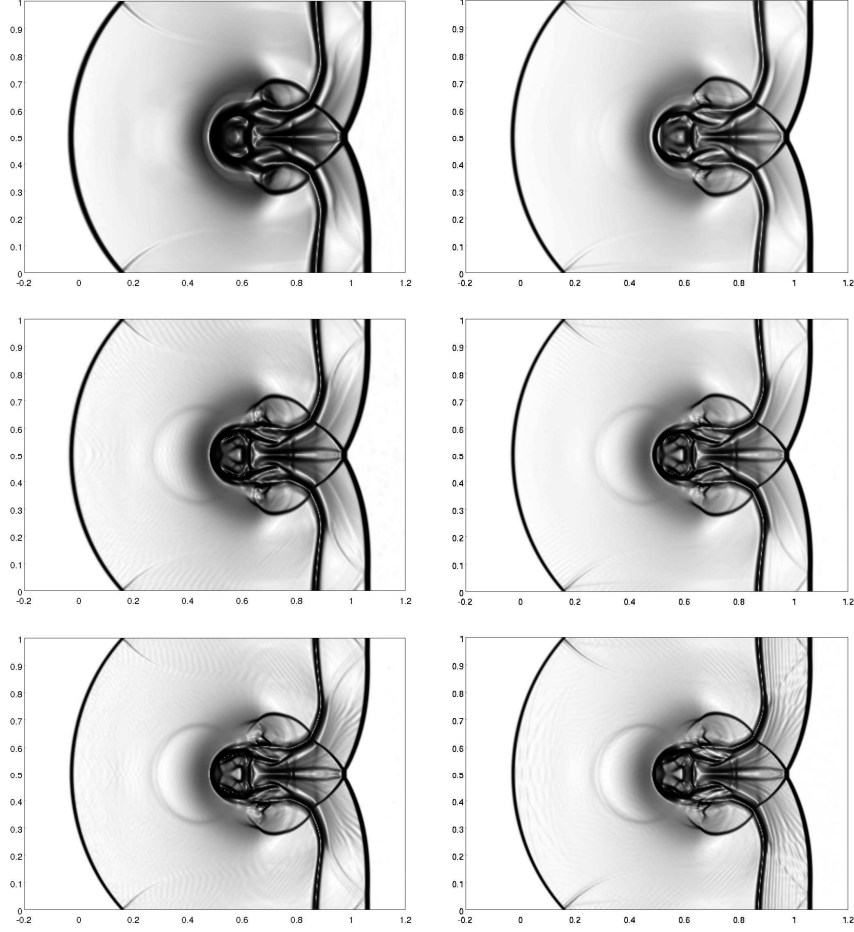


Figure 5.27. Same as Fig. 5.26 except for the magnetic pressure p_m .

- [25] C.Q. Hu and C.-W. Shu. A discontinuous Galerkin finite element method for Hamilton-Jacobi equations. *SIAM J. Sci. Comput.*, 21:666-690, 1999.
- [26] A.V. Koldoba, O.A. Kuznetsov, and G.V. Ustyugova. An approximate Riemann solver for relativistic magnetohydrodynamics. *Mon. Not. R. Astron. Soc.*, 333:932-942, 2002.
- [27] S.S. Komissarov. A Godunov-type scheme for relativistic magnetohydrodynamics. *Mon. Not. R. Astron. Soc.*, 303:343-366, 1999.
- [28] L. Krivodonova. Limiters for high-order discontinuous Galerkin methods. *J. Comput. Phys.*, 226:879-896, 2007.
- [29] O. Lepsky, C.Q. Hu, and C.-W. Shu. Analysis of the discontinuous Galerkin method for Hamilton-Jacobi equations. *Appl. Numer. Math.*, 33:423-434, 2000.
- [30] F.Y. Li and C.-W. Shu. Locally divergence-free discontinuous Galerkin methods for MHD equations. *J. Sci. Comput.*, 22:413-442, 2005.
- [31] F.Y. Li and L.W. Xu. Arbitrary order exactly divergence-free central discontinuous Galerkin methods for ideal MHD equations. *J. Comput. Phys.*, 231:2655-2675, 2012.

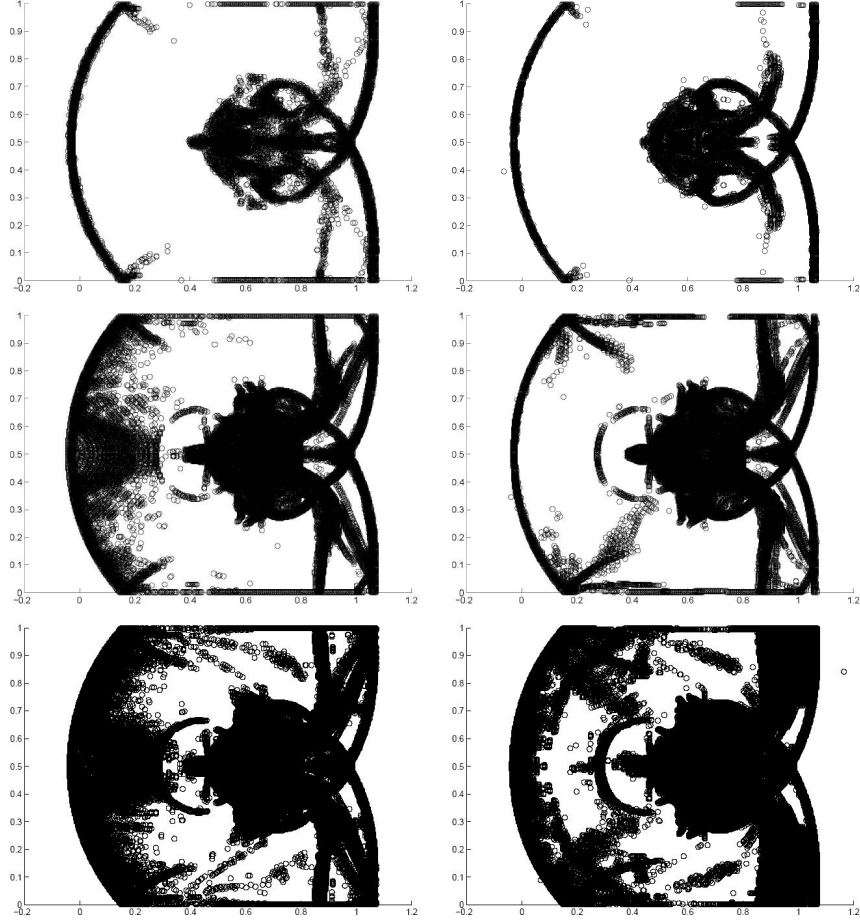


Figure 5.28. Same as Fig. 5.26 except for the “troubled” cells.

- [32] F.Y. Li, L.W. Xu, and S. Yakovlev. Central discontinuous Galerkin methods for ideal MHD equations with the exactly divergence-free magnetic field. *J. Comput. Phys.*, 230:4828-4847, 2011.
- [33] F.Y. Li and S. Yakovlev. A central discontinuous Galerkin method for Hamilton-Jacobi equations. *J. Sci. Comput.*, 45:404-428, 2010.
- [34] Y.J. Liu. Central schemes on overlapping cells. *J. Comput. Phys.*, 209:82-104, 2005.
- [35] Y.J. Liu, C.-W. Shu, E. Tadmor, and M.P. Zhang. Central discontinuous Galerkin methods on overlapping cells with a nonoscillatory hierarchical reconstruction. *SIAM J. Numer. Anal.*, 45:2442-2467, 2007.
- [36] R. Loubère, M. Dumbser, and S. Diot. A new family of high order unstructured MOOD and ADER finite volume schemes for multidimensional systems of hyperbolic conservation laws. *Commun. Comput. Phys.*, 16:718-763, 2014.
- [37] M.M. May and R.H. White. Hydrodynamic calculations of general-relativistic collapse, *Phys. Rev.*, 141:1232-1241, 1966.
- [38] M.M. May and R.H. White. Stellar dynamics and gravitational collapse, in *Methods in*

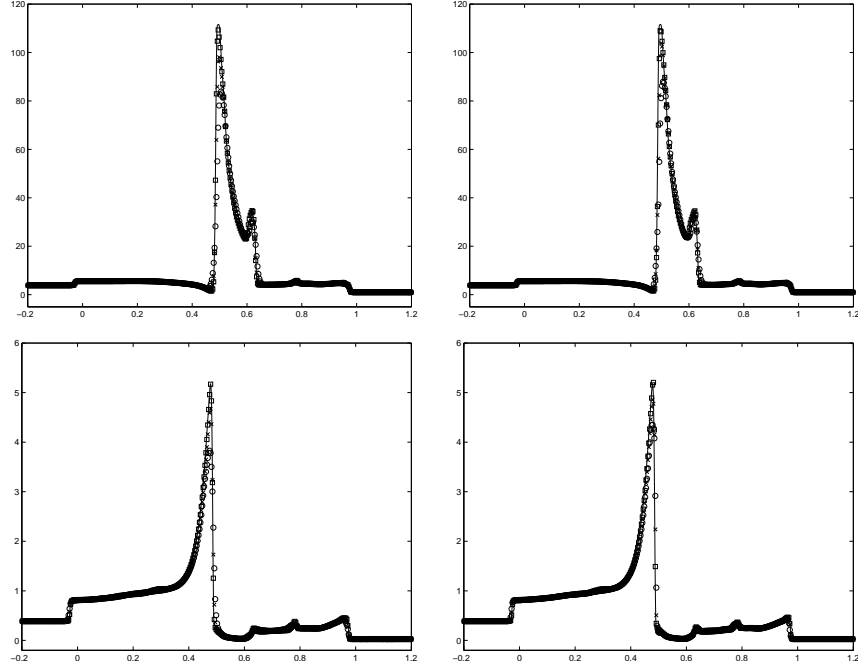


Figure 5.29. Example 5.9: The density ρ (top) and the magnetic pressure p_m (bottom) at $t = 1.2$ along the line $y = 0.5$. The solid line denotes the reference solution obtained by using the MUSCL scheme with 980×700 cells, while the symbols “o”, “x”, and “□” denote the numerical solutions obtained by the P^1 -, P^2 -, and P^3 -based methods with 420×300 cells, respectively. Left: DG methods; right: central DG methods.

Computational Physics, Vol. 7, Astrophysics (B. Alder, S. Fernbach, and M. Rotenberg eds.), Academic Press, 219-258, 1967.

- [39] A. Mignone and G. Bodo. An HLLC Riemann solver for relativistic flows II. magnetohydrodynamics. *Mon. Not. R. Astron. Soc.*, 368:1040-1054, 2006.
- [40] S.C. Noble, C.F. Gammie, J.C. McKinney, and L. Del Zanna. Primitive variable solvers for conservative general relativistic magnetohydrodynamics. *Astrophys. J.*, 641:626-637, 2006.
- [41] K.G. Powell. An approximate Riemann solver for magnetohydrodynamics (that works in more than one dimensions). *ICASE Report No. 94-24, Langley, VA*, 1994.
- [42] S. Qamar and G. Warnecke. A high-order kinetic flux-splitting method for the relativistic magnetohydrodynamics. *J. Comput. Phys.*, 205:182-204, 2005.
- [43] T. Qin, C.-W. Shu and Y. Yang. Bound-preserving discontinuous Galerkin methods for relativistic hydrodynamics. *J. Comput. Phys.*, 315:323-347, 2016.
- [44] J.X. Qiu and C.-W. Shu. Runge-Kutta discontinuous Galerkin method using WENO limiters. *SIAM J. Sci. Comput.*, 26:907-929, 2005.
- [45] W.H. Reed and T.R. Hill. Triangular mesh methods for neutron transport equation. Technical Report LA-UR-73-479, Los Alamos Scientific Laboratory, 1973.

- [46] J.-F. Remacle, J.E. Flaherty, and M.S. Shephard. An adaptive discontinuous Galerkin technique with an orthogonal basis applied to compressible flow problems. *SIAM Rev.*, 45:53-72, 2003.
- [47] J.A. Rossmannith. A high-resolution constrained transport method with adaptive mesh refinement for ideal MHD. *Comput. Phys. Comm.*, 164:128-133, 2004.
- [48] S.H. Shao and H.Z. Tang. Higher-order accurate Runge-Kutta discontinuous Galerkin methods for a nonlinear Dirac model. *Discrete Contin. Dyn. Syst. Ser. B*, 6:623-640, 2006.
- [49] C.-W. Shu. High order weighted essentially nonoscillatory schemes for convection dominated problems. *SIAM Rev.*, 51(2009), 82-126.
- [50] H.Z. Tang and G. Warnecke. A Runge-Kutta discontinuous Galerkin method for the Euler equations. *Computers & Fluids*, 34:375-398, 2005.
- [51] G. Tóth. The $\nabla \cdot \mathbf{B} = 0$ constraint in shock-capturing magnetohydrodynamics codes. *J. Comput. Phys.*, 161:605-652, 2000.
- [52] B. van der Holst, R. Keppens, and Z. Meliani. A multidimensional grid-adaptive relativistic magnetofluid code. *Comput. Phys. Comm.*, 179:617-627, 2008.
- [53] J.R. Wilson. Numerical study of fluid flow in a Kerr space. *Astrophys. J.*, 173:431-438, 1972.
- [54] J.R. Wilson. A numerical method for relativistic hydrodynamics. In L.L. Smarr, editor, *Sources of Gravitational Radiation*, pages 423-446. Cambridge University Press, 1979.
- [55] K.L. Wu and H.Z. Tang. A direct Eulerian GRP scheme for spherically symmetric general relativistic hydrodynamics. *SIAM J. Sci. Comput.*, 38:B458-B489, 2016.
- [56] K.L. Wu and H.Z. Tang. High-order accurate physical-constraints-preserving finite difference WENO schemes for special relativistic hydrodynamics. *J. Comput. Phys.*, 298:539-564, 2015.
- [57] K.L. Wu and H.Z. Tang. Admissible states and physical constraints preserving numerical schemes for special relativistic magnetohydrodynamics. *arXiv:1603.06660*, 2016.
- [58] K.L. Wu and H.Z. Tang. Physical-constraints-preserving central discontinuous Galerkin methods for special relativistic hydrodynamics with a general equation of state. *arXiv:1607.08332*, 2016.
- [59] K.L. Wu and H.Z. Tang. Finite volume local evolution Galerkin method for two-dimensional relativistic hydrodynamics. *J. Comput. Phys.*, 256:277-307, 2014.
- [60] K.L. Wu, Z.C. Yang, and H.Z. Tang. A third-order accurate direct Eulerian GRP scheme for one-dimensional relativistic hydrodynamics. *East Asian J. Appl. Math.*, 4:95-131, 2014.
- [61] Z.C. Yang, P. He, and H.Z. Tang. A direct Eulerian GRP scheme for relativistic hydrodynamics: one-dimensional case. *J. Comput. Phys.*, 230:7964-7987, 2011.

- [62] Z.C. Yang and H.Z. Tang. A direct Eulerian GRP scheme for relativistic hydrodynamics: two-dimensional case. *J. Comput. Phys.*, 231:2116-2139, 2012.
- [63] L. Del Zanna and N. Bucciantini. An efficient shock-capturing central-type scheme for multidimensional relativistic flows I: Hydrodynamics. *Astron. Astrophys.*, 390:1177-1186, 2002.
- [64] L. Del Zanna, N. Bucciantini, and P. Londrillo. An efficient shock-capturing central-type scheme for multidimensional relativistic flows II. Magnetohydrodynamics. *Astron. Astrophys.*, 400:397-413, 2003.
- [65] J. Zhao. *Runge-Kutta discontinuous Galerkin methods for relativistic hydrodynamics and magnetohydrodynamics*. PhD thesis, School of Mathematical Sciences, Peking University, China, 2014.
- [66] J. Zhao and H.Z. Tang. Runge-Kutta discontinuous Galerkin methods with WENO limiter for the special relativistic hydrodynamics. *J. Comput. Phys.*, 24:138-168, 2013.
- [67] J. Zhao and H.Z. Tang. Central Runge-Kutta discontinuous Galerkin methods for the special relativistic hydrodynamics. *arXiv: 1609.06792*, 2016.
- [68] J. Zhu and J.X. Qiu. Runge-Kutta discontinuous Galerkin method using WENO-type limiters: three-dimensional unstructured meshes. *Commun. Comput. Phys.*, 11:985-1005, 2012.
- [69] J. Zhu, J.X. Qiu, C.-W. Shu, and M. Dumbser. Runge-Kutta discontinuous Galerkin method using WENO limiters II: unstructured meshes. *J. Comput. Phys.*, 227:4330-4353, 2008.